Tunnelling and Underground Space Technology 138 (2023) 105175

Contents lists available at ScienceDirect

Tunnelling and Underground Space Technology incorporating Trenchless Technology Research

journal homepage: www.elsevier.com/locate/tust

Response of buried box-shaped road tunnel against internal BLEVE and its damage mitigation

Ruishan Cheng, Wensu Chen *, Hong Hao *, Jingde Li

Center for Infrastructural Monitoring and Protection, School of Civil and Mechanical Engineering, Curtin University, Australia

ARTICLE INFO

Keywords:
Road tunnel
BLEVE
Liquid-filling ratio
Cover depth
Damage mitigation

ABSTRACT

Box-shaped road tunnels have been widely used in urban areas and might face the threats of accidental Boiling Liquid Expansion Vapor Explosions (BLEVEs) due to ever-increasing liquified petroleum transportation. However, very limited study has investigated the response of popularly used buried box-shaped road tunnels (i.e., box-shaped tunnels buried in soil mass) subjected to internal BLEVEs. In this study, the dynamic response of a typical two-cell box-shaped road tunnel buried in soil subjected to internal BLEVEs induced by the burst of a 20 m^3 liquified petroleum gas (LPG) tank is numerically investigated by using LS-DYNA. The results show that the tunnel experiences severe damage under BLEVEs with liquid-filling ratios equal to or more than 65% while it suffers only minor damage with the load carrying capacity not compromised under BLEVE with 50% filled-liquid. The effects of BLEVE occurring locations on the tunnel response are then investigated. It is found that the tunnel subjected to the BLEVE occurring on the lane near middle wall experiences more significant response in general than that away from the middle wall. In addition, to mitigate the tunnel damage under BLEVEs, strengthening soil mass around the tunnel using soil–cement mixture is considered and its performance is examined. An empirical formula is also proposed for the design of using soil–cement mixture to enhance the buried box-shaped tunnel against internal BLEVEs.

1. Introduction

Buried box-shaped road tunnels have been widely used in metropolitan area worldwide to relieve urban traffic congestion on the ground surface (Cheng et al., 2021), such as the Northbridge tunnel in Australia, the Pedder Street tunnel in China, and the Clyde tunnel in UK, as shown in Fig. 1. They are typically excavated in shallow soft grounds or soils, constructed near or beneath above-ground buildings and streets, and functioned as the nexus of urban road systems. Therefore, it is of great significance to study the safety and resilience of box-shaped tunnels under extreme loads.

With ever-increasing urban gas requirements, Liquified Petroleum Gas (LPG) tanks for inter-regional transportation are very likely to pass through buried box-shaped road tunnels to supply oil or gases for urban gasoline-stations and satisfy the commercial and residential consumption requirements (Cheng et al., 2021; van den Berg and Weerheijm, 2006). During transportation, the accidental explosions due to the burst of LPG tanks inside buried box-shaped road tunnels, i.e., Boiling Liquid Expansion Vapor Explosions (BLEVEs) might occur due to various reasons such as vehicle collisions or fire engulfment. A BLEVE is a physical explosion induced by rapid vapor expansion and liquid flashing due to the instantaneous bursting of liquified oil or gas tanks. The characteristics of a BLEVE pressures are different from those from high explosive (HE) explosion (e.g., TNT explosion) and Vapor Cloud Explosion (VCE), which are two types of chemical explosions. The differences in loading characteristics can refer to the handbook of gas explosion (Bjerketvedt et al., 1997) and the CCPS guideline (2011). The potential internal BLEVEs might severely damage buried box-shaped road tunnels and influence the stability of ground surface structures, and thus threatening personnel and property in the vicinity of tunnels (Birk et al., 2007; Cheng et al., 2022b; To et al., 2021). Therefore, it is essential to investigate the performance of buried box-shaped road tunnels under internal explosions associated with transported liquified gases.

Existing studies (Chu et al., 2016; Feldgun et al., 2008; Tiwari et al., 2018; Yu et al., 2015) have investigated the dynamic response of buried road tunnels subjected to internal high explosive (HE) explosions. It has been reported that the behaviour of tunnels subjected to internal HE

* Corresponding authors.
E-mail addresses: wensu.chen@curtin.edu.au (W. Chen), hong.hao@curtin.edu.au (H. Hao).

https://doi.org/10.1016/j.tust.2023.105175
Received 4 November 2022; Received in revised form 4 February 2023; Accepted 19 April 2023
Available online 1 May 2023

explosions is different from that under internal BLEVEs due to significantly different loading characteristics between these two types of explosions (Birk et al., 2007; Cheng et al., 2022a). Compared to HE explosions, BLEVEs with the same energy release usually generate the blast loads with lower overpressure, longer duration, slower pressure rise, and higher impulses (Cheng et al., 2022a). However, only limited studies have investigated the behaviour of tunnels under internal BLEVEs and yet most of them used oversimplified BLEVE load as input in the study. For instance, Vervuurt et al. (2007) numerically investigated the dynamic response of a two-cell box-shaped tunnel subjected to an internal BLEVE loading with an assumed overpressure of 500 kPa. Simplified free-field BLEVE loads with an instantaneous loading rise were utilized in their study. The applied loading profile with an instantaneous pressure rise cannot reflect the actual BLEVE loads in the confined tunnels which consist of multiple peaks owing to wave reflections and non-instantaneous loading rise. Inaccurate application of blast loads is likely to lead to inaccurate predictions of structural response. The authors in the previous study (Cheng et al., 2022a) numerically investigated the response of an arched underground road tunnel surrounded by rock mass subjected to the internal BLEVE induced by the burst of a 20 m^3 LPG tank. However, the performance of popularly-used box-shaped road tunnels buried in soil mass under internal BLEVEs has not been properly investigated yet.

To mitigate the damage of tunnels under explosion, various measures or solutions, e.g., ultra-high-performance concrete (Meng et al., 2020), expandable polystyrene (EPS) concrete (Zhao et al., 2015), and carbon fiber reinforced polymer (CFRP) (Phulari and Goel, 2021) can be considered to replace or enhance conventional concrete of buried tunnels. However, their application in practice might be limited due to high-cost. Soil-cement mixture, i.e., soil treated with cement has been widely applied to enhance the soil strength and stiffness, which can be considered as a mitigation measure due to its easy-to-implement during tunnel construction and operation. The cementitious soil with enhanced strength and stiffness is expected to improve the blast-resistance of tunnels under internal explosions owing to the improved surrounding supports to tunnel structures. In the previous studies (Di et al., 2021; Hu et al., 2003; Nicolini and Nova, 2000), soil–cement mixture was used to enhance and stabilize tunnels constructed in harsh environment, e.g., soft soil, high-weathered rock mass, and highly-dense building area, etc. However, no study has been conducted to evaluate the performance of mixed soil–cement in reducing tunnel response under BLEVEs. In addition, the appropriate soil–cement mixture ratios and the required soil-improvement thicknesses to ensure tunnel safety under BLEVEs are yet to be determined. Therefore, it is essential to investigate the performance of buried road tunnels covered by mixed soil–cement under internal BLEVEs to facilitate the efficient safety assessment and effective blast-resistant designs of road tunnels used for transportation of oil, gas and other explosible chemicals.

In this study, the dynamic response of a typical two-cell box-shaped road tunnel subjected to internal BLEVEs induced by the burst of a 20 m^3 LPG tank is investigated using the finite element software LS-DYNA. The BLEVE loads are simulated by the computational fluid dynamics software FLACS, the accuracy of which in predicting the BLEVE overpressure inside tunnels has been validated in the authors' previous study (Li et al., 2022). The model of reinforced concrete (RC) walls of tunnel has been also previously calibrated by the authors (Cheng et al., 2022a) and is not presented in this study. The model to simulate the response of tunnel surrounded by soil is calibrated with the test results of concrete pipe buried in sandy soil subjected to an internal TNT-equivalence explosion (Bonalumi et al., 2011a; 2011b). With the calibrated model, the effects of tunnel cover depths, liquid-filling ratios in LPG tank, and BLEVE occurring locations inside tunnel on the response of the buried road tunnel are investigated. Moreover, the tunnel responses under BLEVE and its TNT-equivalence explosion are compared to examine the accuracy of the commonly used TNT-equivalence method in BLEVE load predictions for structural response analysis. Finally, soil–cement mixture as a mitigation measure is considered and its performance against BLEVEs is examined.

2. Model development and calibration

To investigate the response of buried road tunnels against internal BLEVEs, a numerical model of a two-cell box-shaped road tunnel surrounded by sandy soil is established and calibrated in this section. LS-DYNA is an advanced general-purpose multi-physics finite element (FE) simulation software package, which has proven good capability for nonlinear transient dynamic analysis of structures and geological media using explicit time integration. However, it cannot directly simulate the process of BLEVE. On the other hand, FLACS as a Computational Fluid Dynamics (CFD) software implemented with BLAST module has been widely used to simulate the process of gas explosions (e.g., BLEVE), including blast wave propagation and overpressure prediction. However, FLACS cannot simulate the structural response under blast loads. Therefore, FLACS is used together with LS-DYNA to calculate tunnel responses. The details are given below.

2.1. Finite element model of buried road tunnel

A box-shaped road tunnel including two vehicle-access cells and a middle evacuation passageway is established, as shown in Fig. 2**(a)**. According to the design guides of road tunnels, i.e., JTG 3370.1–2018 (Ministry of Transport of the People's Republic of China, 2018) and FHWA-NHI-10–034 (US Department of Transportation Federal Highway Administration, 2009), the two vehicle-access cells have the same inner dimension of 10.4 m (horizontal span) × 4.9 m (height) and the evacuation passageway has an inner dimension of 3.2 m (horizontal span) × 4.9 m (height), as shown in Fig. 2**(b)**. Each vehicle-access cell has two lanes with a total width of 7 m. The box-shaped road tunnel is comprised

Fig. 1. Typical buried box-shaped road tunnels in urban area, (a) Northbridge tunnel in Perth, Australia (from website (1)), (b) Pedder Street tunnel in Hong Kong, China (from website (2)), and (c) Clyde-tunnel in Glasgow, UK (from website (3)). (1) https://en.wikipedia.org/wiki/Graham_Farmer_Freeway. (2) https://zh-yue.m.wikipedia.org/wiki/File:Connaught-Road-Central-near-Pedder-Street-Tunnel-West-End.jpg. (3) https://www.reglasgow.com/massive-investment-needed-in-clyde-tunnel-and-approach-roads/.

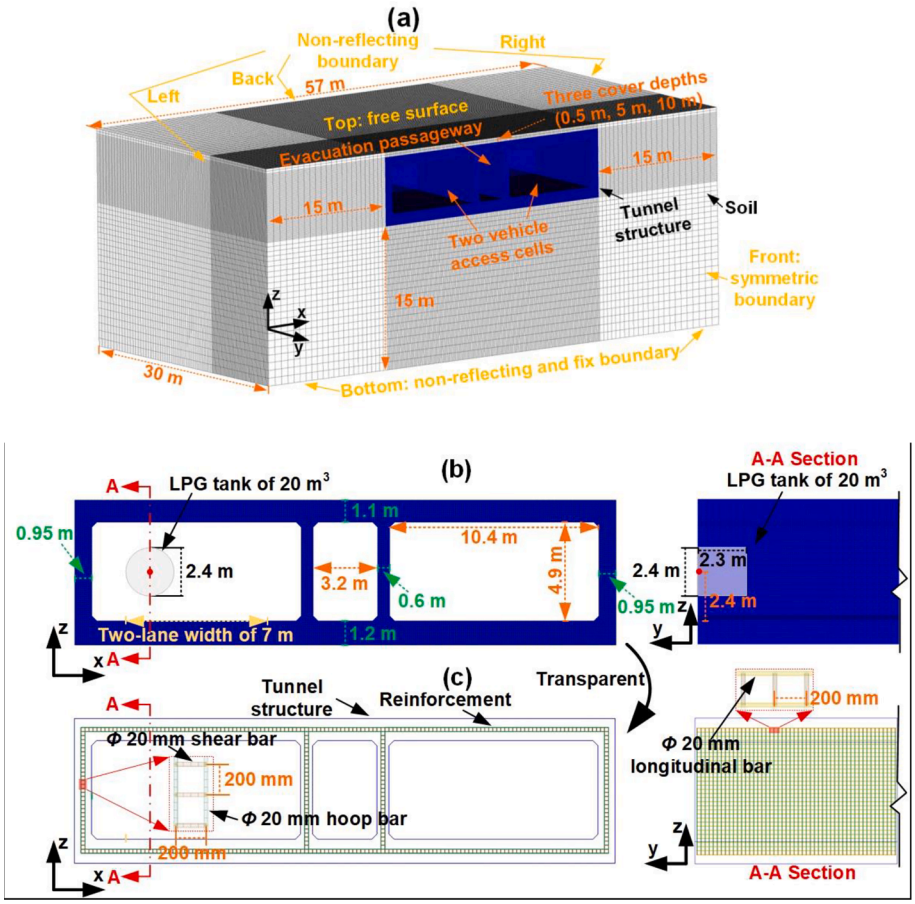

Fig. 2. The numerical model of buried road tunnel. (a) The whole numerical model and boundary conditions, (b) lining configurations, (c) steel reinforcement configurations.

of reinforced concrete (RC) roof slab with a thickness of 1.1 m, RC floor slab with a thickness of 1.2 m, and 0.95 m thick RC sidewall and 0.6 m thick RC middle partition wall, as the East Lake tunnel in China (Yang et al., 2019). The steel rebars including longitudinal, hoop, and shear rebars with an identical diameter of 28 mm are arranged at a spacing of 200 mm for the tunnel walls and slabs, as shown in Fig. 2**(c)**. According to FHWA-NHI-10–034 (US Department of Transportation Federal Highway Administration, 2009), the cover depth of the buried box-shaped road tunnel can vary from 0.5 m to 10 m. In this study, numerical models of the box-shaped road tunnel with three cover depths of 0.5 m, 5 m and 10 m (see Fig. 2**(a)**) are established to investigate the effect of cover depth on tunnel responses under internal BLEVEs.

Boiling Liquid Expansion Vapor Explosions (BLEVEs) induced by the burst of a 20 m^3 liquified petroleum gas (LPG) tank (with a diameter of 2.4 m and length of 4.6 m) are assumed to occur inside the left cell of the box-shaped road tunnel. Fig. 2**(b)** shows the case of LPG tanker driving on the left lane of the left vehicle-access cell. To save computational costs, the numerical model is established as a half symmetric domain by assigning a symmetric boundary to the front surface of the numerical model. The width and length of the model domain are respectively determined as 57 m and 30 m based on the domain convergence study, i.e., the reflected stress wave from the numerical boundary does not interact with the incident stress wave induced by BLEVE at the points of interest. The distance between the box-shaped tunnel and numerical boundary is 15 m as shown in Fig. 2**(a)**. The top surface of the numerical model is assigned as a free boundary to simulate the ground surface, while the non-reflecting boundary condition is assigned to the back, left, right, and bottom surfaces to simulate the infinite domain of soil mass. The fixed boundary is assigned to the bottom surface to prevent the numerical model from moving along the *z* direction under internal explosion loading.

By conducting mesh convergence study, 100 mm solid elements and 50 mm beam elements are respectively determined to mesh the tunnel concrete near BLEVEs and the steel reinforcement. The interaction between the concrete and steel reinforcement is defined by the keyword *CONSTRAINED_BEAM_IN_SOLID in LS-DYNA. To save computational costs, the mesh size of concrete and surrounding soil gradually increases to 600 mm as the distances from the explosion centre increase. The total number of elements varies from 4 million to 4.83 million with the cover depth increasing from 0.5 m to 10 m.

2.2. *BLEVE loads acting on road tunnel*

During the transportation of the 20 m^3 LPG tank, BLEVEs might occur on either lane inside vehicle-access cell of the box-shaped road tunnel. In this section, two scenarios of BLEVE, i.e., BLEVEs occurring on either left or right lanes inside the left vehicle-access cell are respectively simulated using the computational fluid dynamics (CFD) software FLACS. The bursting pressure of the LPG tank is required as the input of BLEVE simulation using FLACS, which is obtained by the energy-based analytical method developed by the authors in the previous study (Li et al., 2022). By inputting the finally-generated bursting pressure into FLACS, the BLEVE inside the tunnel can be simulated by specifying the computational domain, establishing the full-size tunnel model, and setting the location and volume of the assumed LPG tank. The accuracy of FLACS-simulated BLEVE inside the tunnel and the method to calculate the bursting pressure have been validated by the authors in the previous study (Li et al., 2022), which are not given in detail herein for brevity.

The generated BLEVE loads are then directly applied onto the inner wall of the road tunnel built in LS-DYNA to investigate the response of road tunnel and surrounding media. The first 8 m section of the left vehicle-access cell along the longitudinal direction (i.e., the y-direction) in LS-DYNA is divided into 8 segments subjected to BLEVE loads. Each segment is subdivided into 16 parts (i.e., A-P) along the cross-section, as shown in Fig. 3. BLEVE loads are assumed uniform in each part for simplification. No noticeable difference in tunnel response is observed if the cross-section is further divided into more parts (i.e., more than 16). Two keywords, i.e., *Define_Curve and *Load_Segment_Set in LS-DYNA are invoked to apply the BLEVE load at the centre of each part extracted from FLACS onto the corresponding part in LS-DYNA model, which are commonly and popularly used to apply non-LS-DYNA user-defined loads to the numerical model in LS-DYNA due to their ease of operation and high reliability.

In addition, the 20 m^3 LPG tank can be filled with different volume fractions of pressurized liquified gas up to 80% in the tank (Origin-Energy, 2015). In this study, BLEVEs induced by the burst of LPG tank with three percentages of pressurized liquified gas, i.e., 50%, 65%, and 80% are considered. According to Bubbico and Marchini (2008), 50% of the total energy of pressurized liquids and vapours in the tank is likely to be dissipated by vessel deformation, fragments and other energy losses. The remaining energy would contribute to generating BLEVE waves, which in the worst scenario, the source pressures of BLEVE from the 20 m^3 LPG tank with 50%, 65%, and 80% liquified gases in the tank may respectively reach 7.1 MPa, 16.9 MPa, and 32.3 MPa based on the pressure-energy equations given by Li et al. (2022). The BLEVE loads acting on the tunnel structures can be generated by specifying the source pressures of BLEVE. Fig. 4 shows the BLEVE loads applied to different divided areas of tunnel walls under the scenario of 50% liquified gas as an illustrative case.

2.3. Material model

The tunnel structures (i.e., the concrete and the steel rebars) and surrounding soil mass are included in the numerical model. In this study, the concrete and steel rebars are simulated by the Karagozian & Case model (i.e., *MAT_CONCRETE_DAMAGE_REL3) and a piecewise elastic–plastic model (i.e., *MAT_PIECEWISE_LINEAR_PLASTICITY), respectively. The details of the two material models can refer to the LS-DYNA keyword user's manual (Livermore Software, 2020). These two material models have been used in many studies (Cheng et al., 2022a; Qian et al., 2021a; Qian et al., 2021b), which yield reliable prediction of the response of tunnel structures under blast loads. C40 concrete (i.e., the concrete with the compressive strength of 40 MPa) and HRB400 steel (i.e., steel with the yield strength of 400 MPa) are utilized for the tunnel concrete and steel rebars in this study according to the configurations of the East Lake tunnel in China (Yang et al., 2019). Table 1 lists the parameters of the two material models used in this study. The maximum principle strain of 0.15 and failure plastic strain of 0.12 based on Li et al. (2019) are used as the erosion criteria of concrete and steel reinforcement, respectively.

In addition, the Federal Highway Administration (FHWA) soil model (i.e., *MAT_FHWA_SOIL) is employed to simulate the behaviour of sandy soil in this study. The FHWA soil model with a modified Drucker-Prager yield surface has been widely used to investigate the response of soil mass under blast loads (Busch et al., 2016; Lee, 2006; Suazo and Villavicencio, 2018). This material model includes strain hardening, stain softening, strain rate effect, and pore effect. The description of *MAT_FHWA_SOIL can refer to Lewis (2004). Table 2 lists the parameters of *MAT_FHWA_SOIL for the sandy soil used in this study, which are determined based on the experimental results by Busch et al. (2016) and parametric analysis by Lee (2006).

2.4. Model calibration

The tunnel models including tunnel structures and surrounding soil mass are established using LS-DYNA. The model for reinforced concrete (RC) structures of tunnel has been calibrated using testing results of reinforced concrete (RC) panel subjected to a TNT explosion in the authors' previous study (Cheng et al., 2022a), and thus the details are not presented herein to avoid repetition. More details on the calibration of RC structures of tunnel can refer to Cheng et al. (2022a). In this section, the model calibration for the surrounding soil of the tunnel is conducted by modelling the test of a TNT-equivalence explosion inside a concrete pipe buried in sandy soil (Bonalumi et al., 2011a; 2011b). The details are given below.

2.4.1. Test setup and numerical model

Since no test data of explosion inside a box-shaped concrete tunnel buried in soil mass is available, the test on a circular concrete pipe buried in the low-moisture soft sandy soil subjected to the internal detonation of 10 g TNT-equivalence weight is used herein to calibrate the numerical model as this test scenario is similar to a concrete tunnel buried in a soil mass and subjected to an internal explosion. The circular concrete pipe has a length of 26 m, an inner diameter of 1 m, and an outer diameter of 1.17 m (see Fig. 5). The centre of the concrete pipe is located at 2.885 m from the ground surface. The compressive strength of concrete is 30 MPa. A pressure monitoring point is arranged at the upper right side of the concrete pipe along the cross-section of explosion centre

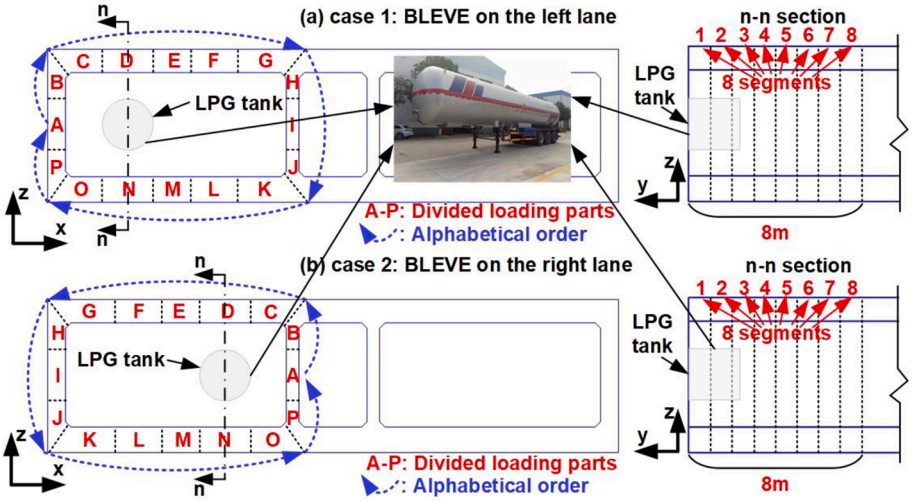

Fig. 3. Schematic diagram of divided BLEVE loading areas for the cases of BLEVE occurring on left and right lanes.

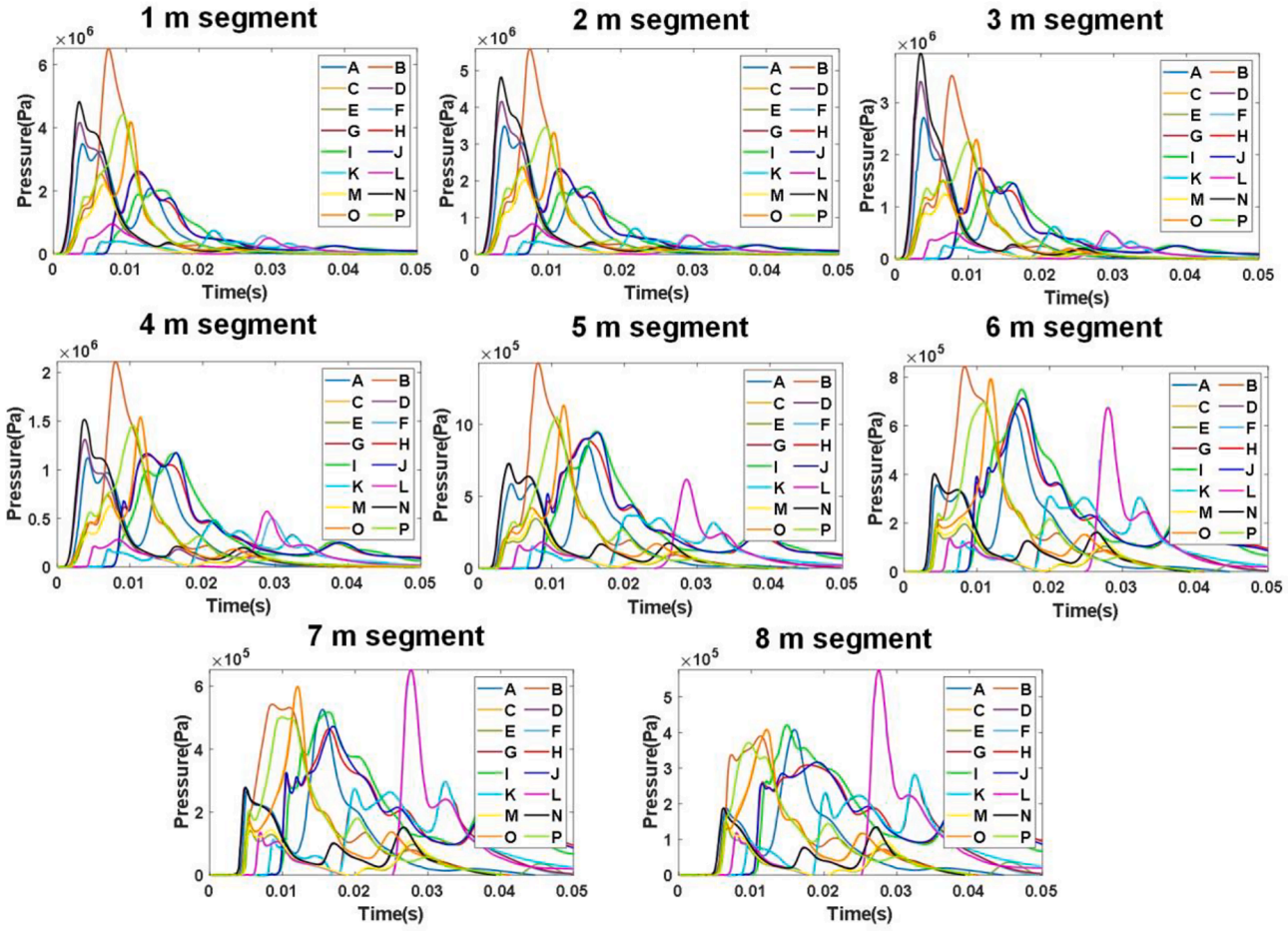

Fig. 4. BLEVE loads applied to different divided areas in the case of 50% liquified gas filled in a 20 m^3 LPG tank.

Table 1
Material model parameters for concrete and steel rebars.

Component	Material model	Relation of stress versus strain	Parameter	Value
Concrete	*MAT_CONCRETE_DAMAGE_REL3	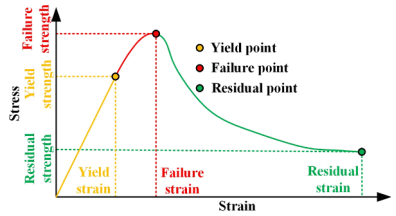	Density Poisson's ratio Compressive strength	2300 kg/m^3 0.2 40 MPa
Steel rebar	*MAT_PIECEWISE_LINEAR_PLASTICITY	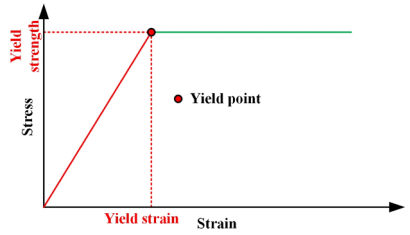	Density Young's modulus Poisson's ratio Yield stress Tangential modulus	7850 kg/m^3 210 GPa 0.3 400 MPa 0 GPa

to record the blast pressure acting on the concrete pipe. Three accelerometers are installed in the sandy soil at 1.285 m, 2.085 m, and 2.885 m from the explosion centre along the vertical direction to record dynamic response of the sandy soil under blast loads. The mechanical properties of the sandy soil used in this test are similar to those in Section 2.3.

According to the test setup, a quarter numerical model including sandy soil mass, concrete pipe, explosive and air inside the concrete pipe is built up, as shown in Fig. 6. The quarter concrete pipe (i.e., a half cylinder with an inner radius of 0.5 m and a longitudinal length of 13 m), the explosive with a quarter dimension of 0.018 m (length) × 0.018 m (width) × 0.02 m (height), and the air inside the concrete pipe are all meshed with sufficiently refined elements, i.e., 0.01 m solid elements. To save computational cost, the surrounding soil mass with the dimension of 13 m (length) × 10 m (width) × 13 m (height) is meshed with the

Table 2
FHWA model parameters for sandy soil (Busch et al., 2016; Lee, 2006).

Type of parameter	Specific parameter	Value	Specific parameter	Value
Basic parameters	Density (kg/m^3)	1630	Specific gravity	2.65
	Nonporous bulk modulus (MPa)	16	Moisture content	0.035
	Shear modulus (MPa)	7.4		
Plasticity parameters	Fraction angle (rad)	0.576	Drucker-Prager Coefficient (KPa)	1.18
	Cohesion (KPa)	15.3	Eccentricity parameter for third invariant effect	1
Pore-water effect parameters	Skeleton bulk modulus (KPa)	1600	Parameters of pore-water effects on bulk modulus	0
	Pore-water density (kg/m^3)	1000	Parameters of pore-water effects on effective pressure	0
Strain hardening parameters	Strain hardening percent	0.25	Strain hardening amount	0.01
Strain softening parameters	Volumetric strain at initial damage	0.1	Void formation energy (J)	10
	Minimum internal friction angle (rad)	0.436		
Strain-rate parameters	Viscoplasticity parameter, V_n	1.1	Viscoplasticity parameter, Gamma	1e-4
Element deletion parameters	Damage level	0.99	Maximum principal failure strain	0.8
Other parameters	Plotting option	3	Maximum number of plasticity iterations	10

element sizes increasing from 0.01 m to 0.5 m with the increased distance from the explosion centre in the pipe. A free boundary is assigned to the top surface of the numerical model, and symmetric boundaries are assigned to the front and left surfaces of the model. The bottom, right, and back surfaces of the model are assigned with non-reflection boundaries. A fixed boundary is also assigned to the bottom surface to prevent the numerical model from moving along the vertical direction. Explosive and air as well as air and concrete pipe share common nodes at their interfaces. *ALE_MULTI-MATERIAL_GROUP is used to define explosive and air as the Arbitrary Lagrangian-Eulerian (ALE) material group. The parameters of *MAT_FHWA_SOIL for the sandy soil are given in Table 2. The concrete pipe is modelled by *MAT_CONCRETE_DAMAGE_REL3. The parameters of material models and equation of state (EOS) for explosive and air are given in Table 3 ((Wei et al., 2009), as shown in Table 3.

2.4.2. Result comparison

Fig. 7 shows the results of measured, simulated and calculated pressure time histories at the pressure monitoring point (see Fig. 5). It is shown that the simulated pressure time history agrees well with the measured and calculated ones with respect to the arrival time, peak pressure, and duration, indicating the built explosive model can well predict explosion pressures inside the concrete pipe. Fig. 8 compares the measured and simulated acceleration time histories at three monitoring points located inside soil mass. It is found that good matches of three acceleration time histories between the simulation and test are achieved with respect to the amplitudes and waveforms. Therefore, it can be concluded that *MAT_FHWA_SOIL can yield good predictions of the response of soil mass subjected to internal explosions.

3. Results and discussion

With the calibrated numerical model, the responses of the box-shaped road tunnel with three cover depths of soil subjected to internal BLEVE are investigated first to study the influences of soil cover depth on the tunnel responses, then the effects of BLEVE condition, i.e., different liquid-filling ratios and BLEVE location on tunnel responses are studied. In addition, to examine the accuracy of using the commonly adopted TNT-equivalence method in predicting the BLEVE loads in structural response analysis, the structural responses of the box-shaped tunnel subjected to internal BLEVE and its TNT-equivalence explosion are compared. The details of the analyses are given below.

3.1. BLEVE-induced response of tunnel with different cover depths of soil

The cover depths of the buried box-shaped road tunnel can vary from 0.5 m to 10 m according to FHWA-NHI-10–034 (US Department of Transportation Federal Highway Administration, 2009). In this section, BLEVE-induced responses of the tunnel with three typical cover depths, i.e., 0.5 m, 5 m, and 10 m are investigated to examine the effect of cover depth on tunnel response. A BLEVE due to the burst of a 20 m^3 LPG tank filled with 80% pressurized liquid is considered to occur on the right lane of the left vehicle-access cell as an extreme scenario.

Fig. 9 shows the structural damage of the box-shaped road tunnel with three cover depths under the internal BLEVE. It can be seen from the top-left and bottom-right views that the structures of left vehicle-

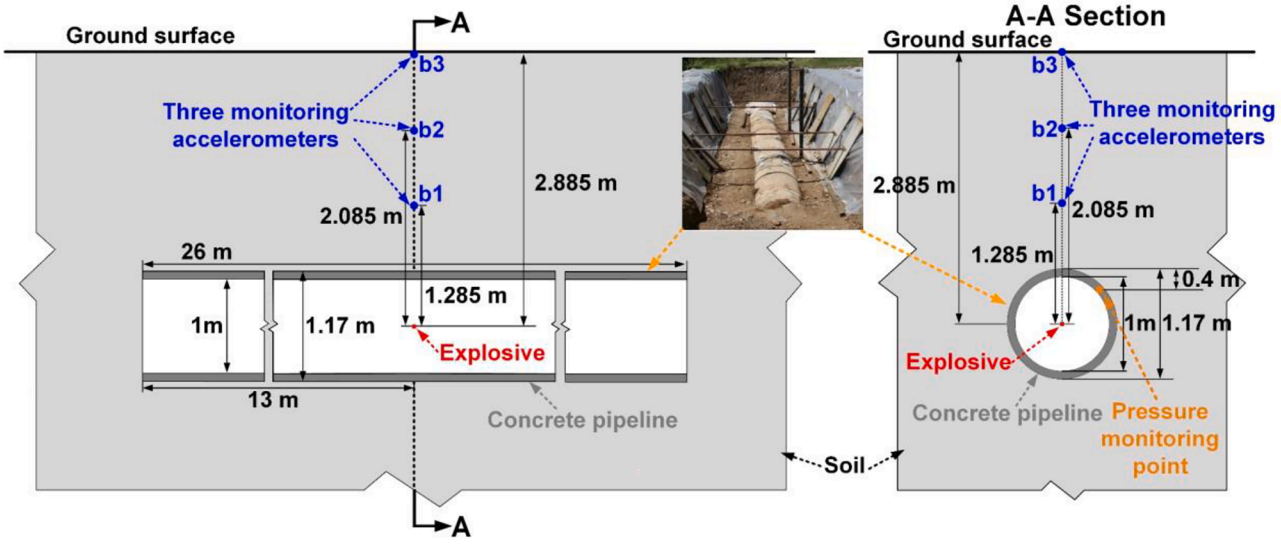

Fig. 5. Test setup of a concrete pipe buried in sandy soil subjected to an internal TNT-equivalence explosion (Bonalumi et al., 2011a; 2011b).

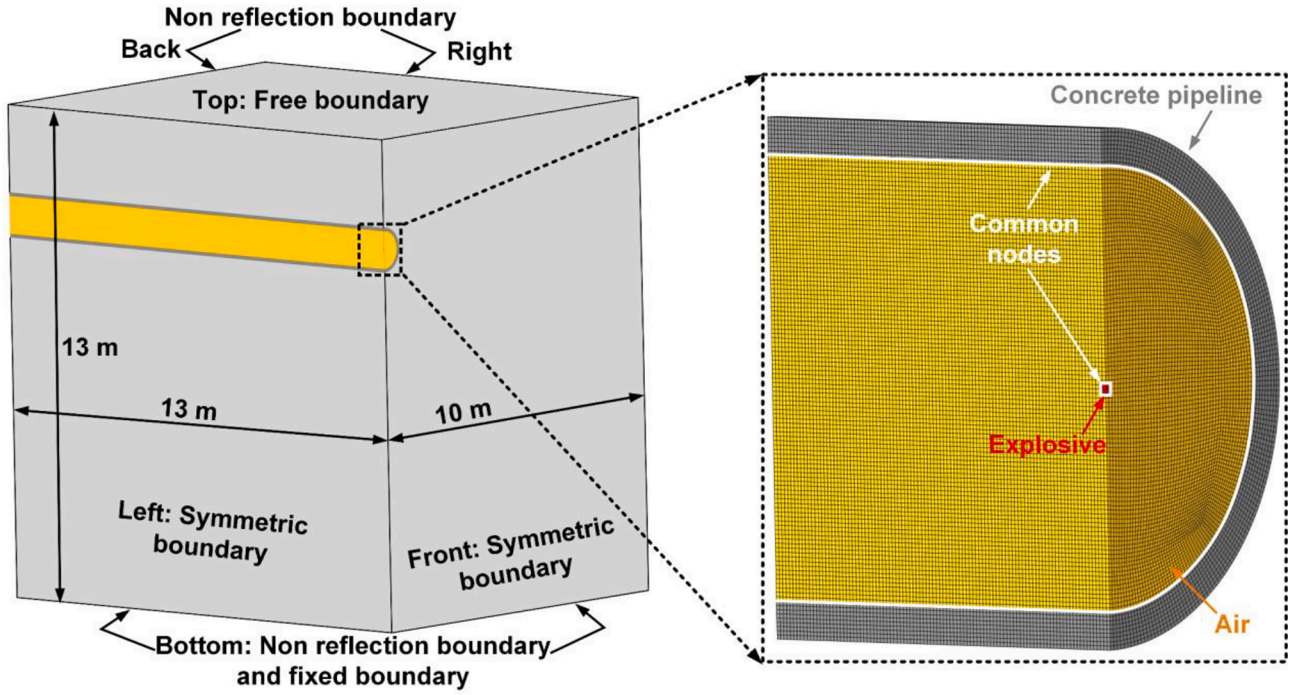

Fig. 6. Numerical model of a concrete pipe buried in sandy soil subjected to an internal TNT-equivalence explosion.

Table 3
Parameters (Wei et al., 2009) and properties of explosive and air.

Component	Material model and EOS	Parameter	Value
TNT explosive	*MAT_HIGH_EXPLOSIVE_BURN	Detonation velocity (m/s)	6930
		Chapman-Jouget pressure (GPa)	21
	*EOS_JWL	Constant A (GPa)	373.8
	$P = A(1-\frac{\omega}{R_1 V})e^{-R_1 V} + B(1-\frac{\omega}{R_2 V})e^{-R_2 V} + \frac{\omega E}{V}$	Constant B (GPa)	3.747
		Constant R_1	4.15
		Constant R_2	0.9
		Constant ω	0.35
		Initial internal energy E_0 (J/m^3)	6×10^9
Air	*MAT_NULL	Density (kg/m^3)	1.255
	*EOS_LINEAR_POLYNOMIAL	Constants C_0, C_1, C_2, C_3, C_6	0
	$P = C_0 + C_1\mu + C_2\mu^2 + C_3\mu^3 + (C_4 + C_5\mu + C_6\mu^2)E_r$	Constants C_4, C_5	0.4
		Initial internal energy E_{r0} (J/m^3)	2.5×10^5

Note: P, V, E and μ are hydrostatic pressure, relative volume, internal energy of explosive per unit volume, and compression parameter, respectively.

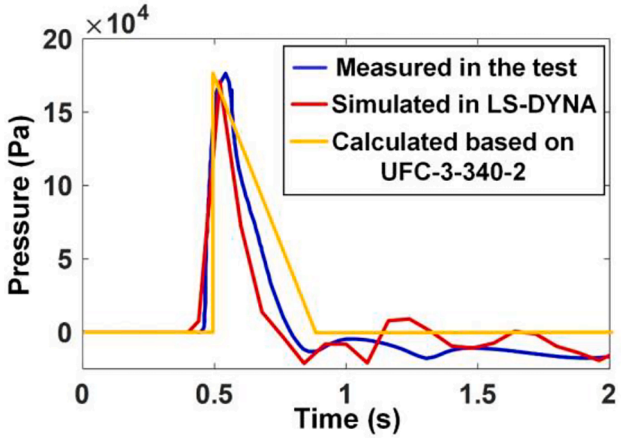

Fig. 7. Comparisons of measured (Bonalumi et al., 2011b), simulated and calculated (US Department of Defense, 2008) pressure time histories at the pressure monitoring point.

access cell in the three cases experience severe damage and the right vehicle-access cell is also damaged due to the action of BLEVE-induced stress waves. As observed from the front view, the left mid-wall near BLEVE in the three cases is completely detached from the roof and floor slabs, and moves a certain distance to the right. The detached range of the left mid-wall along the longitudinal direction are similar under three cover depths, i.e., approximate 7.4 m near the roof slab and 5.4 m near the floor slab. The roof slabs in all three cases experience severe cracking near the connection between the roof slab and the left mid-wall. The crack runs through the thickness of the roof slab (i.e., named as through crack) near the connection in the case of 0.5 m cover depth and has a length of approximate 1.8 m along the longitudinal direction of the tunnel (see enlarged view of the roof slab in Fig. 9**(a)**). Meanwhile, steel rebars in the roof slab with 0.5 m soil cover depth also rupture within the range of 1.2 m along the longitudinal direction of the tunnel. The results indicate that under 0.5 m cover depth, the roof slab at least in the first 1.2 m longitudinal section fails, i.e., loses load-carrying capability under the internal BLEVE. Moreover, the cracks between the roof slab and the left mid-wall in the cases of 5 m and 10 m soil cover depths do not run through the thickness of the roof slab, and no rupture of steel rebars in the roof slab occurs in both cases (see Fig. 9**(b) and (c)**). These results indicate that a thick cover depth up to 10 m is beneficial to reducing the tunnel damage caused by internal explosions. This is because although a thicker cover depth imposes larger gravity load on tunnel structure, it also provides better constraints to the roof slab and larger inertial resistance, therefore leading to smaller roof slab deformation and damage. However, it should be noted that this observation is valid only up to the cover depth of 10 m. A previous study (Cheng et al., 2022c) found that a very deep cover depth may also reduce the explosion resistance capacity of underground tunnels because of the larger gravity

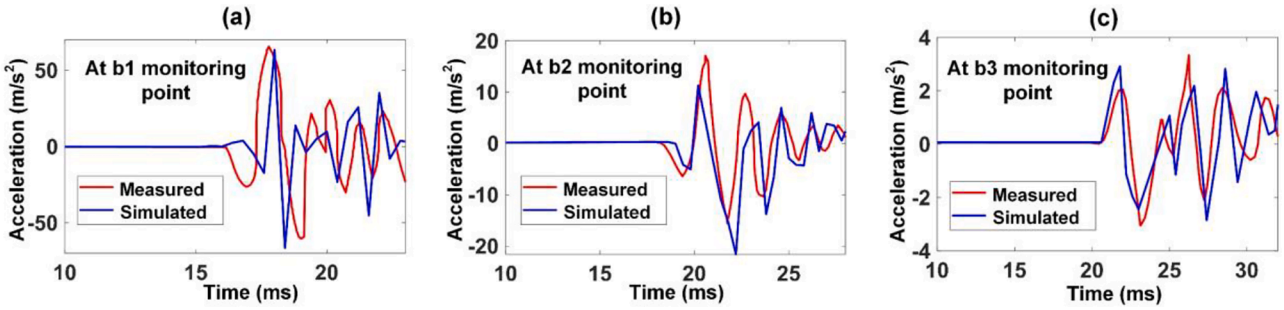

Fig. 8. Comparisons of measured (Bonalumi et al., 2011a) and simulated acceleration time histories at (a) 1.285 m, (b) 2.085 m, and (c) 2.885 m from the explosion centre.

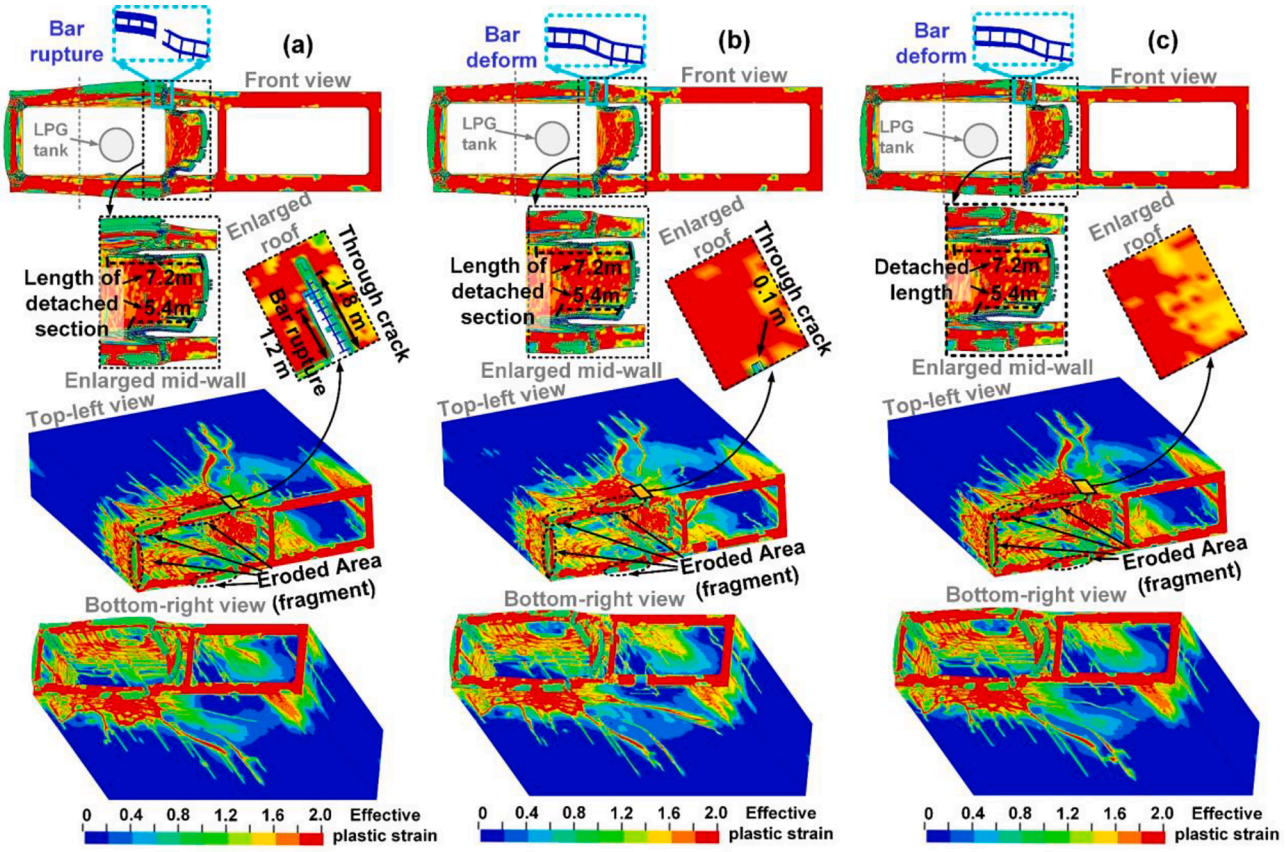

Fig. 9. BLEVE-induced damage of tunnel structures with three cover depths of (a) 0.5 m, (b) 5 m, and (c) 10 m.

load on the tunnel structure. In addition, the left sidewall and floor slab in the cases of 0.5 m, 5 m, and 10 m soil cover depths all experience the through cracks near their connections, but the steel rebars of these walls and slabs are not ruptured. Furthermore, as observed from the top-left views, the eroded areas (i.e., source of fragments) on the left sidewall, roof slab, and floor slab reduce when the cover depth increases from 0.5 m to 5 m. However, very minor variation of eroded area is observed when the cover depth increases from 5 m to 10 m.

To quantitatively reveal the effect of tunnel cover depth on tunnel response under internal BLEVE, BLEVE-induced strain energies of tunnel structures with three cover depths are compared in Fig. 10. It is noted that the strain energy and damage state of tunnel structures given in this study are mainly for the concrete of tunnel structure. The strain energies of the tunnel first decrease from 13 MJ to 11.2 MJ with the cover depth increased from 0.5 m to 5 m, and then slightly increase to 11.6 MJ when the cover depth is 10 m. It is because increasing the tunnel cover depth from 0.5 m to 5 m can better constrain the outward deformation of the roof slab subjected to the internal BLEVE. However, the further-increased soil weight with the cover depth increased from 5 m to 10 m can generate higher static stress in the buried tunnel structure and thus slightly increases the strain energy of the tunnel. The results show that tunnel structures with 5 m soil cover depth experience the least significant BLEVE-induced tunnel response among the cases with soil cover depths of 0.5 m, 5 m, and 10 m.

Fig. 11 shows the peak displacement profiles of the left sidewall, left mid-wall, roof slab, and floor slab in the first 8 m along the longitudinal direction of the tunnel with different cover depths. It can be seen that the peak displacements of the roof with 0.5 m soil cover depth are significantly higher than the ones with 5 m and 10 m cover depths. It is because steel rebars in the roof with 0.5 m soil cover depth rupture during BLEVE loading (see Fig. 9**(a)**). Therefore, the roof with a 0.5 m soil cover depth is prone to be pushed outwards under internal BLEVE due to less constraints of steel bars on the roof deformation. In addition, peak displacement profiles for other tunnel structural components (i.e., left

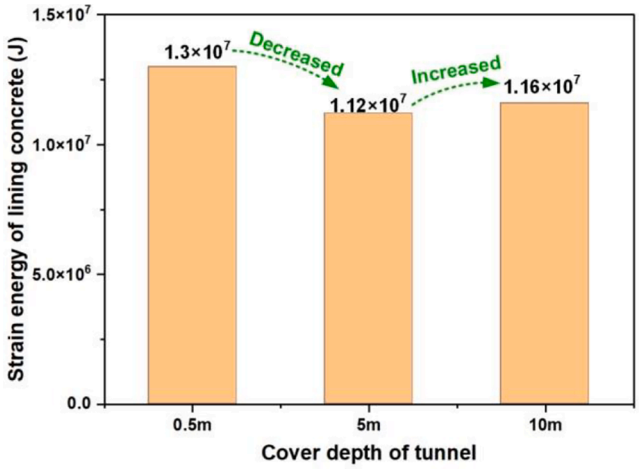

Fig. 10. BLEVE-induced strain energies of tunnel structures with three cover depths.

mid-wall, left sidewall, and floor slab) are similar among the three cases (i.e., the cases of 0.5 m, 5 m, and 10 m cover depths). With the cover depths increased from 0.5 m to 10 m, the increase in static pressure on roof slab owing to the soil self-weight (i.e., approximately 0.16 MPa) is much lower than the BLEVE overpressure (i.e., approximately 17 MPa at the roof slab above the centre of BLEVE with 80% liquid filled tank). Therefore, the influences of soil cover depth on the responses of the sidewall, mid-wall, and floor slab are not prominent as compared to those of BLEVE loads.

To evaluate damage levels of tunnel structural components, the damage criteria of the reinforced concrete (RC) slab based on support rotations as specified in UFC 3–340-02 (US Department of Defense, 2008) are used herein. In UFC 3–340-02 (US Department of Defense, 2008), the allowable maximum support rotations (i.e., support rotations of structural failure) for the RC slab with laced (e.g., spiral-link) and non-laced (e.g., single-leg) shear reinforcement are limited to 12° and 6°, respectively. In this study, single-leg shear reinforcement is used, as shown in Fig. 2**(c)**. Therefore, three damage levels, i.e., slight damage with support rotations not greater than 2°, medium damage with support rotations of 2°-6°, and severe damage greater than 6° are specified as given in Table 4. It should be noted that the previous studies (Ouyang et al., 2020; Qian et al., 2021a; Qian et al., 2021b) also employed these damage criteria to evaluate tunnel damage under blast loads and yield reliable damage classification.

Fig. 12 shows the maximum support rotations of tunnel structural components at different cross-sections of the first 8 m in the longitudinal direction of the tunnel with three soil cover depths. The support rotations of a tunnel structural component (e.g., the roof slab) are calculated based on the differences between the maximum displacement and the displacement at either end of the component divided by their corresponding horizontal distances, as shown in Fig. 12 (d). The larger support rotation is determined as the maximum support rotation of the

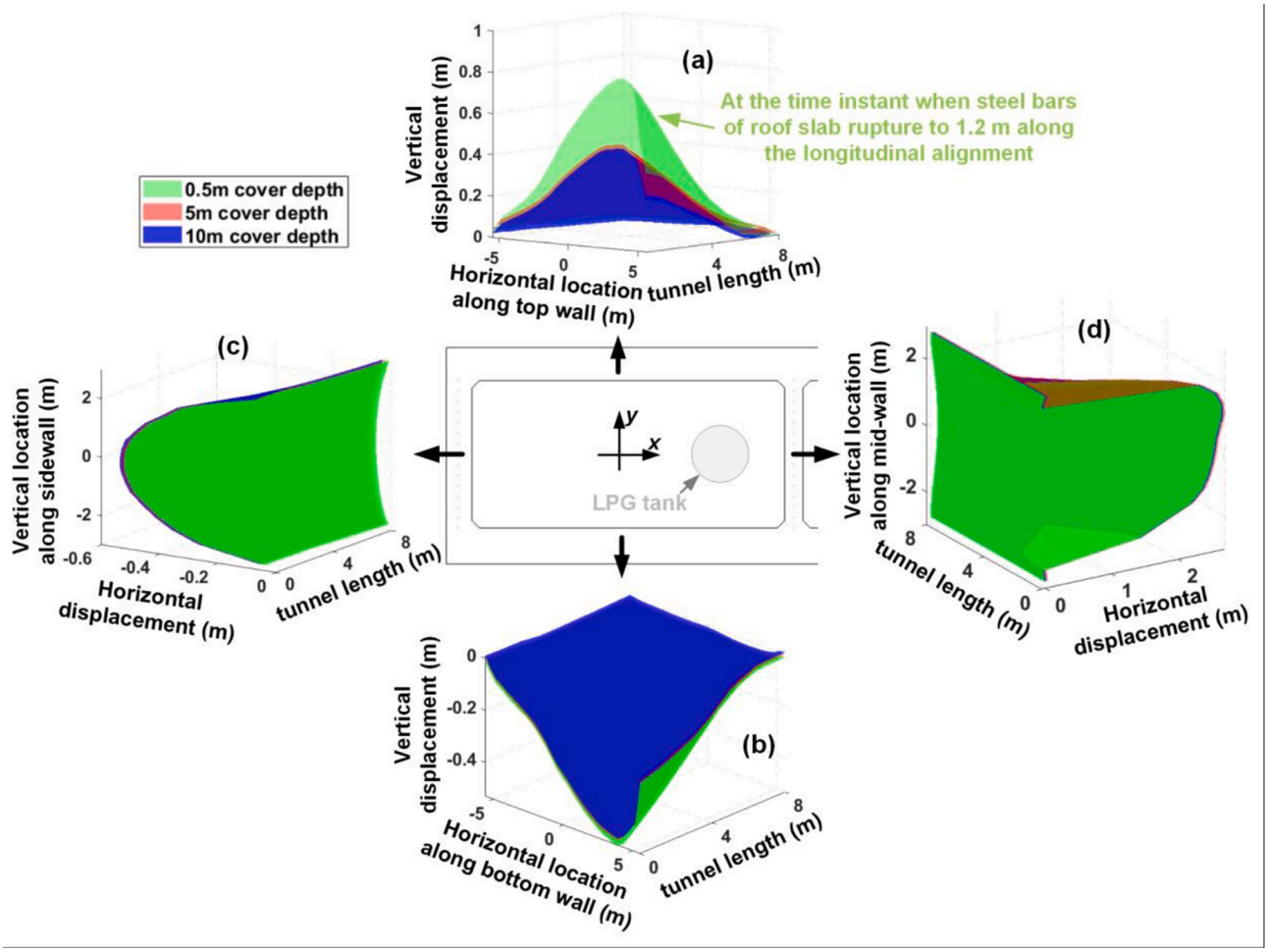

Fig. 11. BLEVE-induced peak displacement profiles of (a) roof slab, (b) floor slab, (c) sidewall, and (d) mid-wall of the first 8 m in the longitudinal section of tunnel with different soil cover depths. Note: Displacements in the case of 0.5 m cover depth are obtained when the rupture range of steel rebars of the roof slab reaches 1.2 m along the longitudinal direction of the tunnel (i.e., at 10 ms after steel rebars of the roof slab start to rupture).

Table 4
Damage criteria based on support rotations specified in UFC 3–340-02 (US Department of Defense, 2008).

Damage index	Slight damage	Medium damage	Severe damage (i.e., failure)
Support rotationθ	$\theta \leq 2^\circ$	$2^\circ < \theta \leq 6^\circ$	$\theta > 6^\circ$

component. It is noted that the maximum support rotations of the mid-wall are not given since the mid-wall is severely damaged in the three cases of cover depths and the failure ranges can be well identified based on the damage patterns, as shown in Fig. 9. As shown in Fig. 12**(a)**, the maximum support rotations of the roof slab in the first 3 m along the longitudinal direction exceed 6° (i.e., the limit of medium and severe damage) under 0.5 m soil cover depths. That is to say, the roof within the first 3 m range along the longitudinal direction fails or loses load-carrying capability (i.e., collapse) in the case of 0.5 m soil cover depth. The severe damage (i.e., the maximum support rotations over 6°) is limited in the 1 m range along the longitudinal direction in the cases with 5 m and 10 m soil cover depth. Moreover, the ranges of the sidewall and floor slab experiencing severe damage (i.e., failure) are respectively also limited to the 3 m and 1 m range in the longitudinal direction for the three cases of soil cover depth (see Fig. 12**(b) and (c)**).

Based on the support rotations and damage patterns, it can be concluded that the tunnels with three cover depths around the BLEVE location all experience severe damage, i.e., the collapse of the partial roof slab and the mid-wall between the two traffic cells. The failure ranges of tunnel structures are significantly influenced by the variation of cover depth. The tunnel with thin soil cover (e.g., 0.5 m) experiences a wider range of collapse under the internal BLEVE of 80% pressurized liquid filled in a 20 m^3 LPG tank due to insufficient soil constraints on tunnel deformations. In addition, the tunnel with larger soil cover depth (e.g., 10 m) also experiences severe damage under the internal BLEVE due to the BLEVE-induced stress combined with the soil self-weight-induced static stress. Therefore, the influences of cover depth on the tunnel responses need to be considered in assessing the performance and design of buried tunnels.

3.2. Effects of the liquid-filling ratio on BLEVE-induced tunnel response

In reality, the 20 m^3 LPG tank given in Section 2 can be filled with different fractions of pressurized liquid up to 80%. In this section, the BLEVEs induced by the burst of the LPG tank filled with three ratios of pressurized liquid, i.e., 80%, 65%, and 50% are considered and simulated using FLACS. In the worst scenario, the source pressures of BLEVEs with these three liquid-filling ratios in the tank can reach 32.3 MPa, 16.9 MPa, and 7.1 MPa, respectively. The BLEVE loads acting on the tunnel wall can be extracted from the FLACS simulation and applied to the inner surface of the tunnel wall in LS-DYNA, as described in Section 2.2. In this section, the BLEVE occurring on the right lane of left vehicle-access cell of the tunnel with 0.5 m cover depth is used for the study.

Fig. 13 shows the structural damage of tunnel subjected to BLEVEs induced by the burst of the LPG tank filled with 80%, 65%, and 50% pressurized liquid. It can be seen that the damage level (i.e., damage region and eroded area) of tunnel significantly decreases with the decreased liquid-filling ratios in the tank. As observed from the front view, the sections of left mid-wall near BLEVE in the cases of 80% and 65% liquid-filling ratios are detached from the floor and roof slabs and move a certain distance to the right. The range of damage in the longitudinal direction (see enlarged views of mid-wall in Fig. 13**(a) and (b)**) and pushed distance (see the bottom-right views in Fig. 13**(a) and**

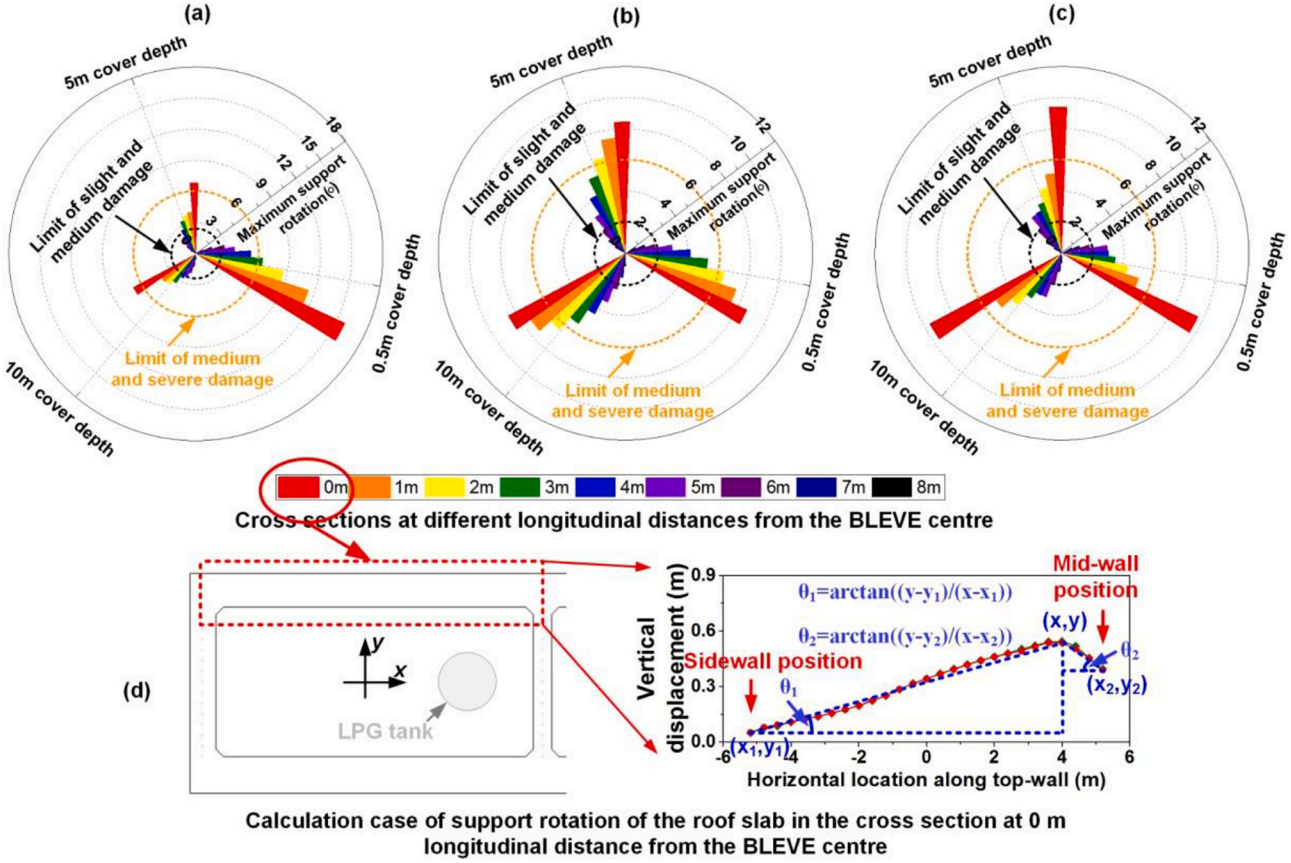

Fig. 12. BLEVE-induced maximum support rotations of (a) roof slab, (b) left sidewall, and (c) floor slab at different cross-sections of the first 8 m longitudinal section of the tunnel with different soil cover depths, and (d) schematic diagram of support rotation calculation.

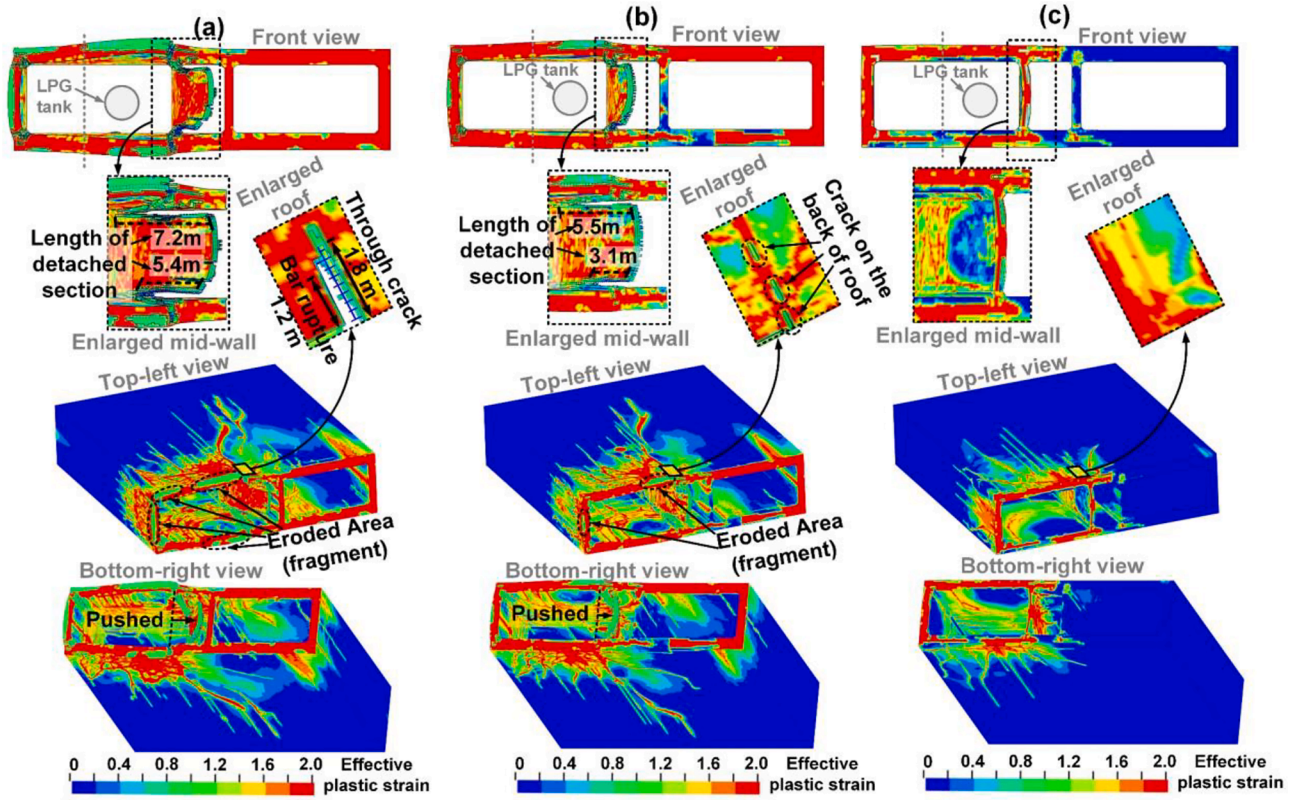

Fig. 13. Damage of tunnel structures subjected to BLEVEs induced by the burst of the LPG tank filled with pressurized liquid of (a) 80%, (b) 65%, and (c) 50%.

(b)) of the detached section of the left mid-wall significantly decrease with the liquid-filling ratio reducing from 80% to 65%. In addition, the left mid-wall in the case of 50% liquid-filling ratio remains integrated with the floor and roof slabs but deforms outward to a certain extent (see the front view in Fig. 13**(c)**). The roof slab, left sidewall, and floor slab near the BLEVE in the case of 80% liquid-filling ratio experience complete damage with through cracks, and the roof slab in the 1.2 m range in the longitudinal direction loses load-carrying capability (i.e., collapses) due to the rupture of steel rebars in the roof slab, as shown in Fig. 13 (a). However, these tunnel structures in another two cases do not experience the through cracks (see the front views in Fig. 13**(b) and (c)**). To quantitatively reveal the effect of liquid-filling ratios in the tank on BLEVE-induced tunnel responses, the ratios of damaged concrete under BLEVEs in the cases of tank with 80%, 65%, and 50% filled liquid are compared in Fig. 14**(a)**. The ratios of damaged concrete in the cases of tank with 65% and 50% filled liquid respectively decrease by 17.42% and 65.92% as compared with that of the tank with 80% filled liquid. The above results are mainly attributed to the decreased BLEVE loads with the reduced liquid-filling ratios, as shown in Fig. 14**(b)**.

To determine the damage levels of tunnel structures under the BLEVEs with different liquid-filling ratios, the peak displacement profiles and the maximum support rotations of tunnel structures in the 8 m

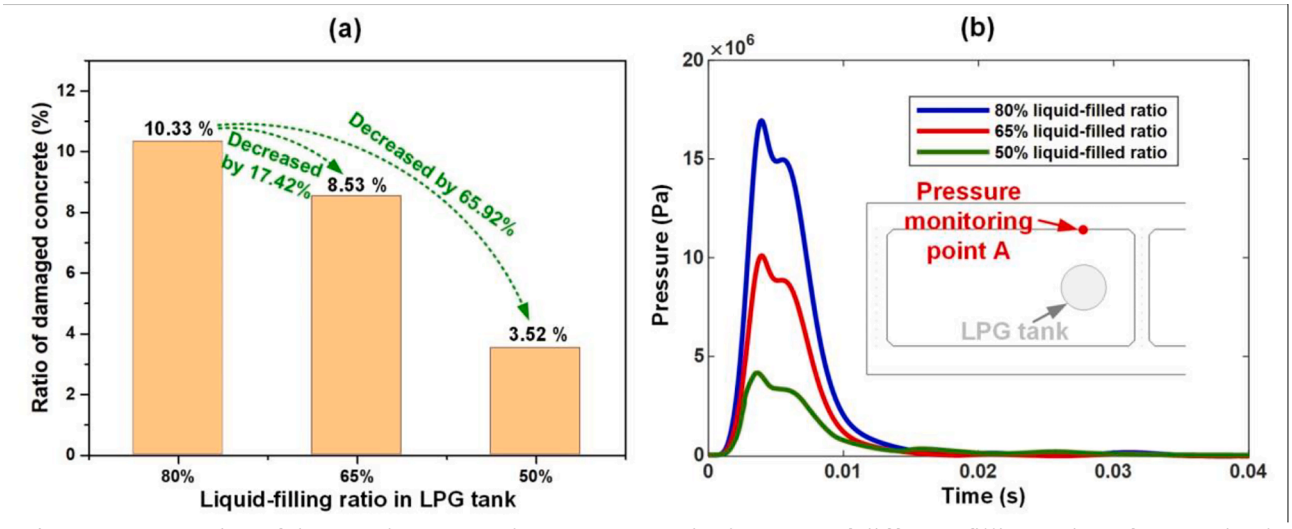

Fig. 14. (a) Ratios of damaged concrete due to BLEVEs in the cases of different filling ratios of pressurized liquid and (b) the corresponding pressure time histories at pressure monitoring point A on the roof.

range along the longitudinal direction for the cases of different liquid-filling ratios are obtained and compared in Fig. 15. It is worth noting that the maximum support rotations of the mid-wall in the cases of 80% and 65% liquid-filling ratios are not given since the mid-wall in the two cases collapses and the ranges of collapse in the longitudinal direction can be identified by damage patterns, as shown in Fig. 13. According to the support rotations for different damage levels listed in Table 4, the roof slab, left sidewall, and floor slab in the case of 80% filled liquid experience severe damage (i.e., the maximum support rotation greater than 6°). That is, certain range of these structural components in the longitudinal direction completely fail or lose load-carrying capability. The loss of load-carrying capacity of the roof slab and left side wall is within 3 m range in this case while the corresponding one of the floor slab is within 1 m range (see Fig. 15**(e)**). Moreover, the roof slab in the case of 65% filled liquid experiences very severe damage (i.e., collapses) in the 1 m range along the longitudinal direction but no severe damage occurs on the left mid-wall and floor slab (see Fig. 15**(f)**). When the liquid-filling ratio is decreased to 50%, the tunnel structures only experience medium-to-slight damage (see Fig. 15**(g)**). The results show that the tunnel structures remain standing without collapse and keep

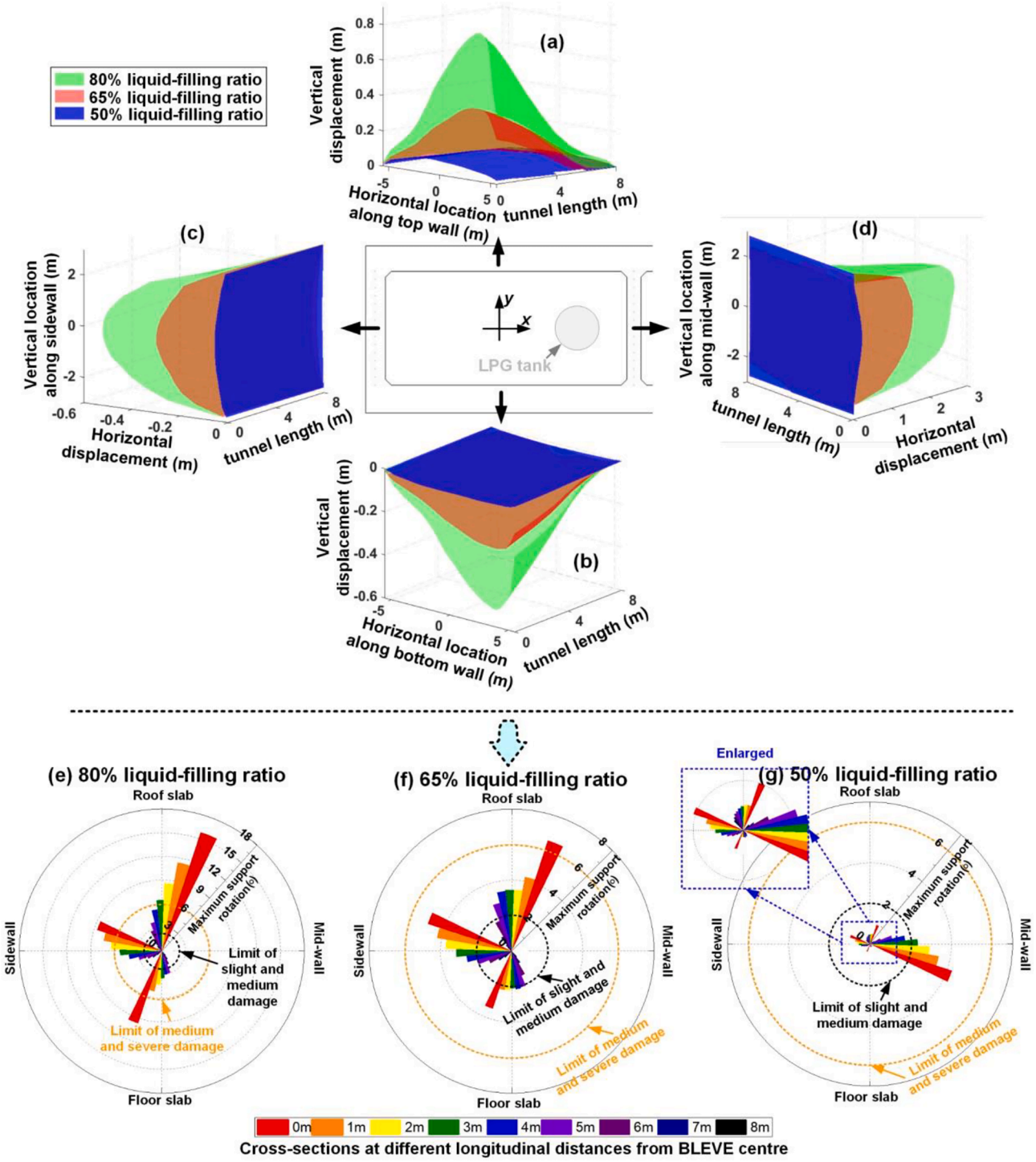

Fig. 15. BLEVE-induced peak displacement profiles of (a) roof slab, (b) floor slab, (c) sidewall, and (d) mid-wall in the cases of different liquid-filling ratios and (e-f) corresponding maximum support rotations.

certain level of load-carrying capability under the BLEVE induced by the burst of the tank filled with 50% pressurized liquid. Therefore, to ensure the safety of the buried tunnel, it is suggested that the liquid-filling ratios need be determined through a proper risk assessment taking into consideration the BLEVE loads and tunnel structural responses.

3.3. Effects of BLEVE location on tunnel response

The LPG tank might drive on either lane inside tunnel if the LPG tank (e.g., the LPG tank filled with 50% liquid) is allowed to pass through the tunnel. Therefore, BLEVEs may occur on either lane inside tunnel during transportation of the LPG tank, which can cause different tunnel responses. In this section, the tunnel responses induced by BLEVEs occurring on the right and left lanes inside the left vehicle-access cell are investigated to suggest the driving lane for the LPG tank inside tunnel. The response of the tunnel with 0.5 m cover depth subjected to internal BLEVEs induced by the burst of the LPG tank filled with 50% pressurized liquid is examined as an illustrative case.

Fig. 16 shows the structural damage of the tunnel subjected to BLEVEs occurring on the right and left lanes of the left vehicle-access cell. It can be seen that the overall damage under the BLEVE occurring on the right lane is more severe than that of BLEVE occurring on the left lane. As observed from the front view, the damage areas of tunnel under the BLEVE occurring on the right lane are wider than those of BLEVE on the left lane. Strain energies of tunnel structures given in Fig. 17 show that the tunnel response under the BLEVE occurring on the right lane is more severe than that of BLEVE on the left lane. It is because the deformation of the left mid-wall under the BLEVE occurring on the right lane is larger than that of BLEVE on the left lane, while the deformation of other tunnel structural components (e.g., the left sidewall) has less difference between the two cases with BLEVE occurring on the right and left lanes, as shown in Fig. 18**(a)-(d)**.

To evaluate the damage levels of tunnel structures subjected to

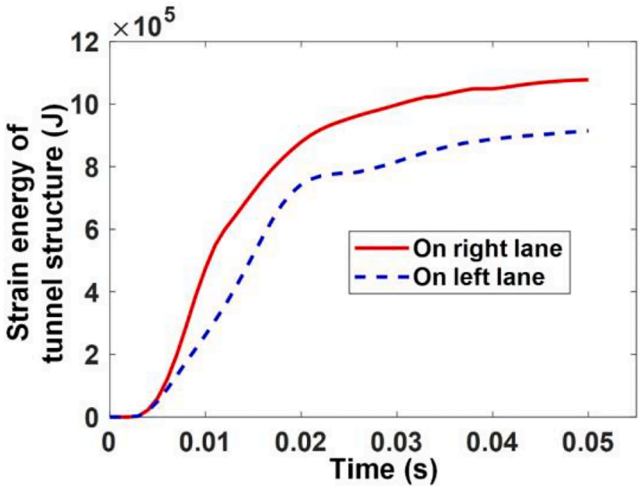

Fig. 17. Strain energy time histories of tunnel structures subjected to BLEVEs occurring on the right and left lanes of the left vehicle-access cell.

BLEVEs occurring on the right and left lanes, Fig. 18**(e)** shows BLEVE-induced maximum support rotations of different tunnel structural components at the cross-section of BLEVE centre under the two cases. Maximum support rotations at other cross-sections are not compared because tunnel structures are not severely damaged (i.e., with the maximum support rotation less than 6°) under the BLEVE of tank with 50% filled liquid. Based on the damage criteria given in Table 4, the roof slab, left sidewall, and floor slab at the cross-section of BLEVE centre subjected to the BLEVE occurring on the right lane experience slight damage. Meanwhile, the left mid-wall in this case has a maximum support rotation of 4.2°, which is classified as medium damage. However, all structural components of tunnel subjected to the BLEVE

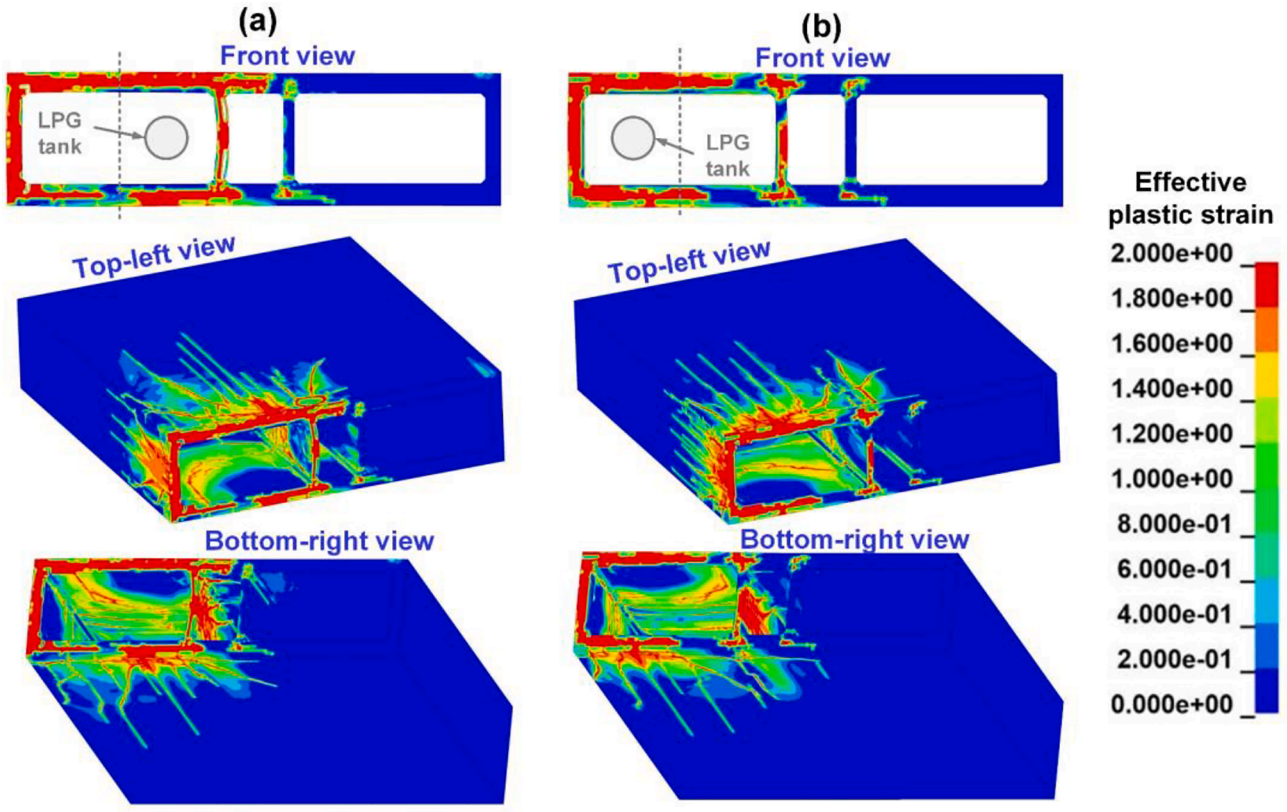

Fig. 16. The structural damage of tunnel subjected to BLEVEs occurring on the (a) right and (b) left lane of the left vehicle-access cell.

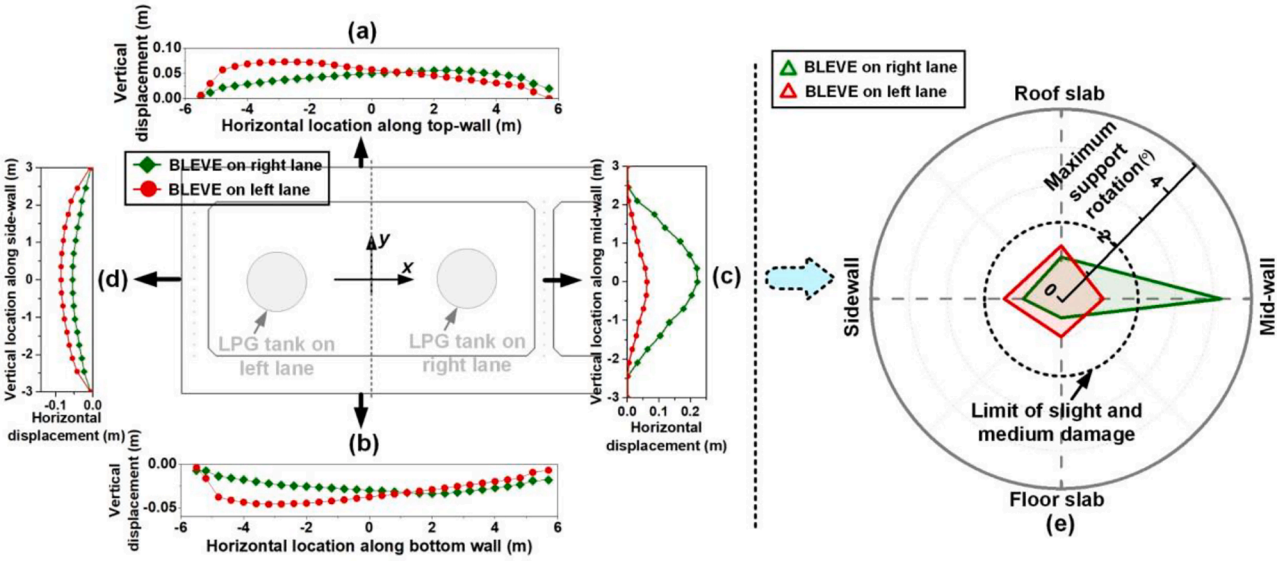

Fig. 18. Peak displacement distribution of (a) roof slab, (b) floor slab, (c) mid-wall, and (d) sidewall at the cross-section of BLEVE centre under BLEVEs occurring on the right and left lane of the left vehicle-access cell and (e) the corresponding maximum support rotations.

occurring on the left lane have the support rotations less than 2°, which is classified as slight damage. Therefore, the LPG tank is suggested to drive on the lane away from the middle partition wall of tunnel to ensure less damage once the internal BLEVE occurs.

3.4. Comparison of tunnel response under BLEVE and its TNT-equivalence explosion

In engineering practice and design, BLEVE loads are often approximated using simplified approaches such as TNT-equivalence method, TNO Multi-Energy method and Baker-Strehlow-Tang method (Lea, 2002). Amongst, the TNT-equivalence method is very commonly used since it is relatively straightforward for engineers. However, using the TNT-equivalence method might lead to inaccurate prediction on the BLEVE loads for structural analysis and design. In this section, the responses of tunnel with 0.5 m cover depth under BLEVE loads and TNT-equivalence explosion loads are compared. The BLEVE is induced by the burst of the LPG tank filled with 50% liquified gas and occurs on the left lane of the left cell.

The TNT-equivalence method proposed by Prugh (1991) is adopted herein to convert the BLEVE energy into a TNT-equivalence weight. Its detailed calculation and parameter acquisition procedures have been presented in the authors' previous study (Cheng et al., 2022a) and therefore are not repeated herein. A TNT weight of 150 kg is derived equivalent to the BLEVE considered in this section. Fig. 19 shows the tunnel model under the TNT equivalence explosion. Half of the TNT with the dimension of 0.3 m (width) × 0.3 m (height) × 0.5 m (length) and the air between the explosive and tunnel structures are established as the Arbitrary Lagrangian-Eulerian (ALE) material group. The TNT explosive is located at the same location as the BLEVE centre. The TNT explosive, air and tunnel structures share common nodes at their respective interfaces. After conducting mesh convergence test, solid elements with the size of 100 mm are determined to mesh the air and explosive inside the tunnel by considering computational efficiency and accuracy. The material models and EOS of the TNT explosive and air are listed in Table 3. Other configurations of the model are kept the same as those in Section 2.1. It is noted that the accuracy of BLEVE simulated by FLACS has been validated in the authors' previous studies (Li et al., 2022) by comparing simulated BLEVE pressure time histories with the experimental data from Birk et al. (2007) and the empirical curves from van den Berg et al. (2006). The model to simulate TNT explosion has been also calibrated in Section 2.4 by comparing simulated TNT explosion loads with the measured one and the calculated one based on UFC3-340–2. Therefore, it is deemed that the simulated BLEVE loads and TNT-

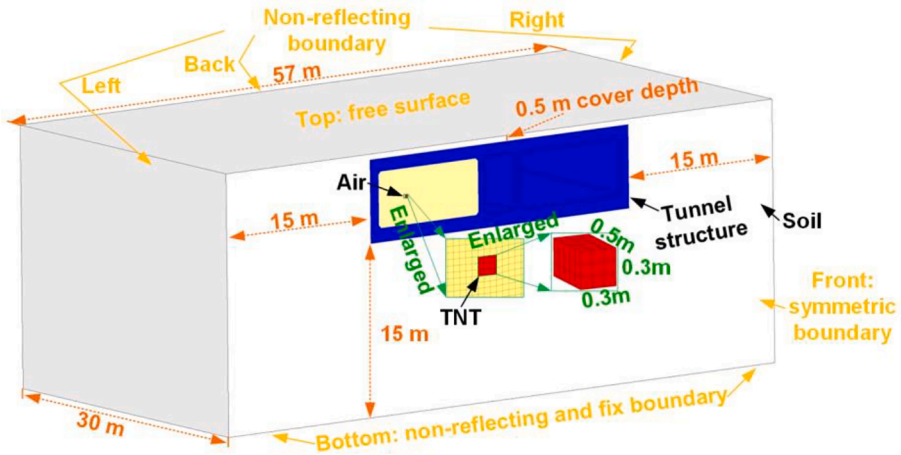

Fig. 19. The tunnel model under TNT-equivalence explosion.

equivalence explosion loads are reliable and accurate.

Fig. 20 shows the structural damage of the tunnel subjected to the BLEVE and its TNT-equivalence explosion. It can be found that the tunnel damage under the TNT-equivalence explosion is less severe than that of the BLEVE. Strain energies of tunnel structures given in Fig. 21**(a)** also show that the TNT explosion-induced tunnel response is lower than that of BLEVE. That is to say, using the TNT equivalence method to predict BLEVE loads underestimates the response of buried road tunnel (i.e., the tunnel surrounded by soil mass) subjected to the internal BLEVE. It is mainly attributed to the difference between BLEVE loads and TNT-equivalence explosion loads. As shown in Fig. 21**(b)**, the TNT-equivalence explosion can generate blast loads with faster rising time, shorter duration, high peak pressure, and lower impulse as compared to the BLEVE. Therefore, TNT-equivalence loads with the lower impulse can induce less deformation of the tunnel structures surrounded by soil mass than BLEVE loads. However, the deformation of the tunnel structures subjected to internal BLEVEs may be well restrained with increased properties of surrounding geological media (e.g., from soil mass to rock mass). In this situation, since peak pressures of TNT explosion loads are higher than BLEVE loads, the TNT-equivalence explosion is likely to induce more severe damage to tunnel structures surrounded by the enhanced geological media than the BLEVE, as observed in the authors' previous studies (Cheng et al., 2022a, c). It is worth noting that the impulse difference between the two explosion loads with the same energy release is attributed to different blasting wave velocities. Impulse (I) is calculated as the integration of force and time. Energy (E) or work is expressed as the integration of force and distance. The relationship between impulse and energy is given as $I = f(E/v)$, where v is the blast wave velocity and f is the mapping function from E/v to I. TNT explosion with the same energy release as BLEVE can generate higher blasting wave velocity, resulting in the blast waves with lower impulse, as shown in Fig. 21**(b)**. In addition, The response of tunnel structures depends on loading characteristics, tunnel structural properties, and the action of geological media around the tunnel.

4. Damage mitigation measure by using soil–cement mixture

As investigated in Section 3, the road tunnel used in this study can be severely damaged under the BLEVEs from a 20 m3 LPG tank filled with 80% and 65% liquified gases. Therefore, to ensure the safety of buried road tunnels against the potential BLEVEs induced by the burst of LPG tank with high liquid-filling ratios, effective measure is needed to mitigate damage. Compared to the inner structures (e.g., the mid-walls) of box-shaped road tunnel, it is more critical to prevent main structures (i.e., the roof slabs, floor slabs and sidewalls) of box-shaped road tunnel from severe damage since main structures support adjacent above-ground structures. In this section, using the soil–cement mixture, i.e., the soil improved by the addition of Ordinary Portland Cement (OPC) is considered as a damage mitigation measure of main structures against internal BLEVEs. In practice, the soil–cement mixture has been widely employed to stabilize tunnels (Di et al., 2021; Fan et al., 2018) due to its significantly improved performance (e.g., enhanced strength and stiffness) of surrounding soil treated by adding cement. The improved soil around tunnel is expected to better constrain the deformation of tunnel structures under internal BLEVEs, which is thus investigated in this section. It should be noted that the roof slab of the tunnel is supported by two mid-walls and two sidewalls. As observed from the simulation, the detachment of a mid-wall from the roof slab has a limited influence on the stability of the roof slab due to the support of two sidewalls and another mid-wall. Using the soil–cement mixture can not only mitigate the response of the roof slab, but also improve the blast resistance of two sidewalls, which can thus ensure sufficient support to the roof slab after experiencing the BLEVE. Therefore, the collapse possibility of the tunnel structures can be greatly reduced with the tunnel surrounding soil improved by cement. The box-shaped road tunnel with a 10 m cover depth subjected to an extreme BLEVE, i.e., an internal BLEVE due to the burst of LPG tank filled with 80% liquified gas experiences severe damage, as observed in Section 3.1. Therefore, this case (see Fig. 22) is utilized to examine the effectiveness of using soil–cement mixture to mitigate tunnel damage under BLEVEs. Three thicknesses of improved soil layer (i.e., 0.5 m, 1 m, and 2 m) and three typical ratios of mixed soil–cement by volume (i.e., 10:0.1, 10:0.45, and 10:0.8) are considered

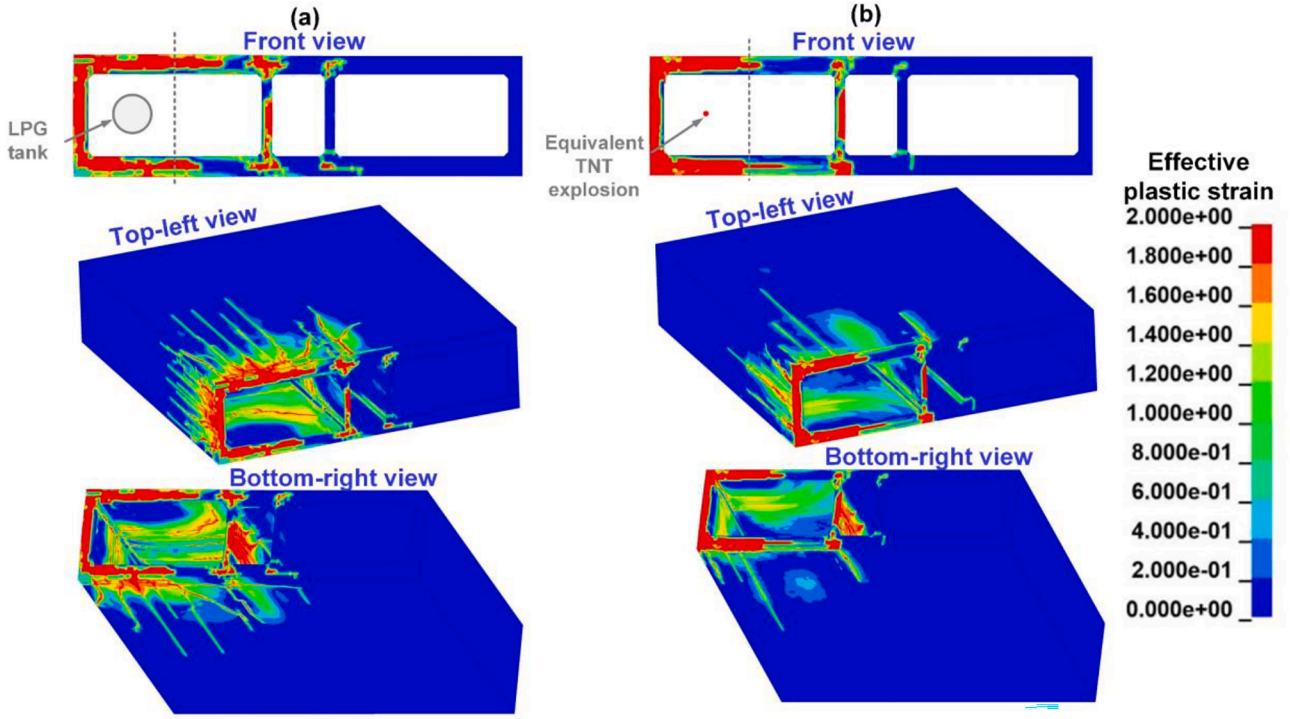

Fig. 20. Structural damage of the tunnel subjected to (a) BLEVE and (b) its TNT-equivalence explosion.

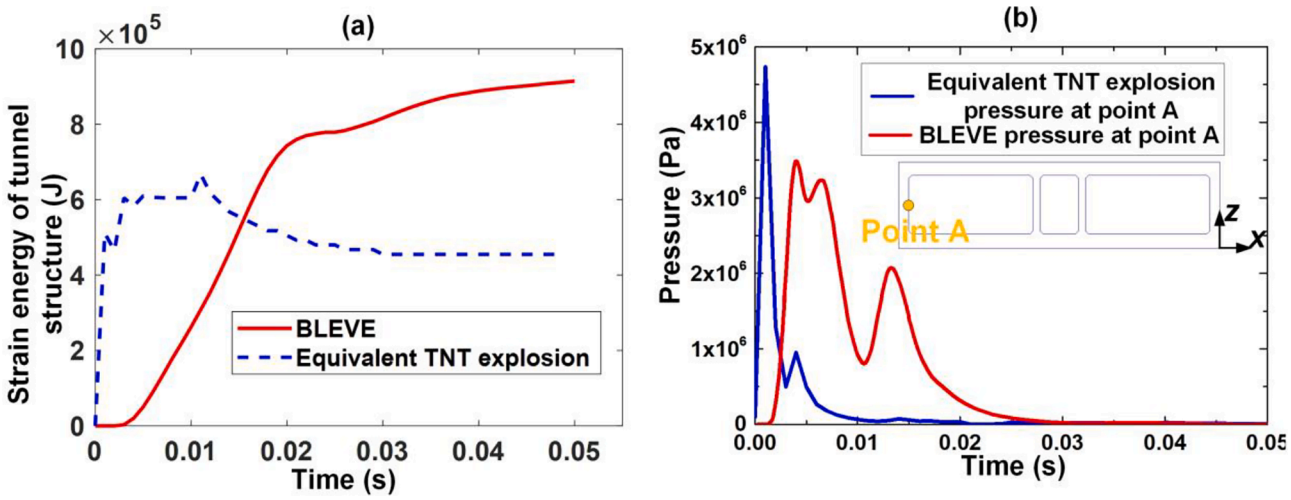

Fig. 21. (a) strain energy time histories of tunnel structures and (b) pressure time histories at monitoring point A (i.e., at the middle of the left sidewall along the explosion centre) under a BLEVE and its TNT-equivalence explosion.

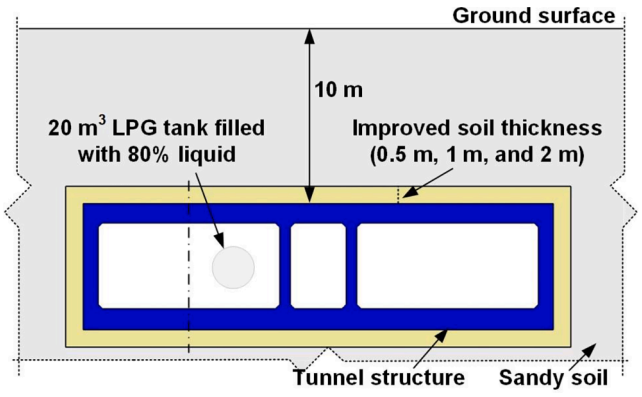

Fig. 22. Simulated case of buried road tunnel surrounded by improved soil subjected to an internal BLEVE.

to examine their mitigation effectiveness. *MAT_FHWA_SOIL in LS-DYNA is employed to simulate the improved soil. The mechanical and physical properties of the improved soil can vary with changing soil–cement mixed ratios. Therefore, the parameters of *MAT_FHWA_SOIL significantly influencing the improved soil with different mixed soil–cement ratios (see Table 5) are calculated based on the empirical relations given in the studies (Consoli et al., 2007; Fan et al., 2018; Lee, 2006). The remaining parameters of *MAT_FHWA_SOIL are set the same as given in Table 2.

4.1. Effects of the improved soil layer thickness on tunnel response

Fig. 23 shows the BLEVE-induced damage of tunnel structures surrounded by three thicknesses (i.e., 0.5 m, 1 m, and 2 m) of improved soil layer with soil–cement ratio of 10:0.8. It can be seen that the damage regions (i.e., red area) of tunnel structures reduce with the increased thickness of improved soil layer. It is because the deformation of tunnel structures under the internal BLEVE can be better constrained by the increased thickness of improved soil layer due to the increased stiffness and strength of the improved soil layer. Meanwhile, the eroded areas (i.e., source of fragments) on the outer surfaces of tunnel structures (i.e., the interfaces between tunnel structures and surrounding soil) gradually increases with the increase of soil-improvement thickness. It may be due to the increased compressive action between the interfaces of tunnel structures and surrounding soil, which is caused by the increased inertia effect of improved soil.

Table 5
Parameters of *MAT_FHWA_SOIL for the improved soil with different soil–cement ratios (Consoli et al., 2007; Fan et al., 2018; Lee, 2006).

Specific parameter	Soil-cement volume ratio		
	10:0.1	10:0.45	10:0.8
	Cement as percentages of soil by weight		
	0.9%	4%	7%
Specific gravity	2.65	2.67	2.69
Density (kg/m^3)	1628	1622	1616
Fraction angle (rad)	0.628	0.628	0.628
Minimum internal friction angle (rad)	0.471	0.471	0.471
Cohesion (KPa)	107	307	437
Nonporous bulk modulus (MPa)	100	184	217
Shear modulus (MPa)	49	90	106
Drucker-Prager Coefficient (KPa)	7.4	21	30
Skeleton bulk modulus (MPa)	10	18.4	21.7
Strain hardening amount	0.07	0.12	0.14
Viscoplasticity parameter, V_n	0.16	0.09	0.08

Note: The specific gravity and density are calculated according to the porosity and the volume ratio of soil and cement; The cohesion, shear modulus, and nonporous bulk modulus are calculated based on empirical formulae given in Fan et al. (2018), which are established as the functions of the uniaxial compressive strength (UCS) of mixed soil–cement; The UCS is calculated based on the empirical formula developed by Consoli et al. (2017) as the functions of the porosity and the soil–cement volume ratio. The remaining parameters in Table 5 are calculated and integrated from Lee (2006). The specific formulae and parameter determination can refer to the above-mentioned studies and are not given in the present study for brevity.

To determine the effectiveness of soil-improvement thickness on preventing severe damage of tunnel main structures (i.e., left sidewall, roof slab, and floor slab) under the BLEVE, their peak displacement and maximum support rotations at the cross-section of BLEVE centre (i.e., the cross-section experiencing the most severe damage) for the cases of three soil-improvement thicknesses are given in Fig. 24. It can be seen that the deformation of tunnel structures decreases with the increased thickness of improved soil layer. The support rotations of the roof slab and floor slab are similar for the cases with various soil-improvement thicknesses. It is because the blast load acting on the floor slab is higher than that on the roof slab, while the floor slab is thicker than the roof slab and floor slab is more constrained by the soil mass underneath the tunnel. In the cases with soil-improvement thicknesses of 1 m and 2 m, the maximum support rotations of tunnel structures are less than 6°. That is, tunnel structures in these two cases do not experience severe

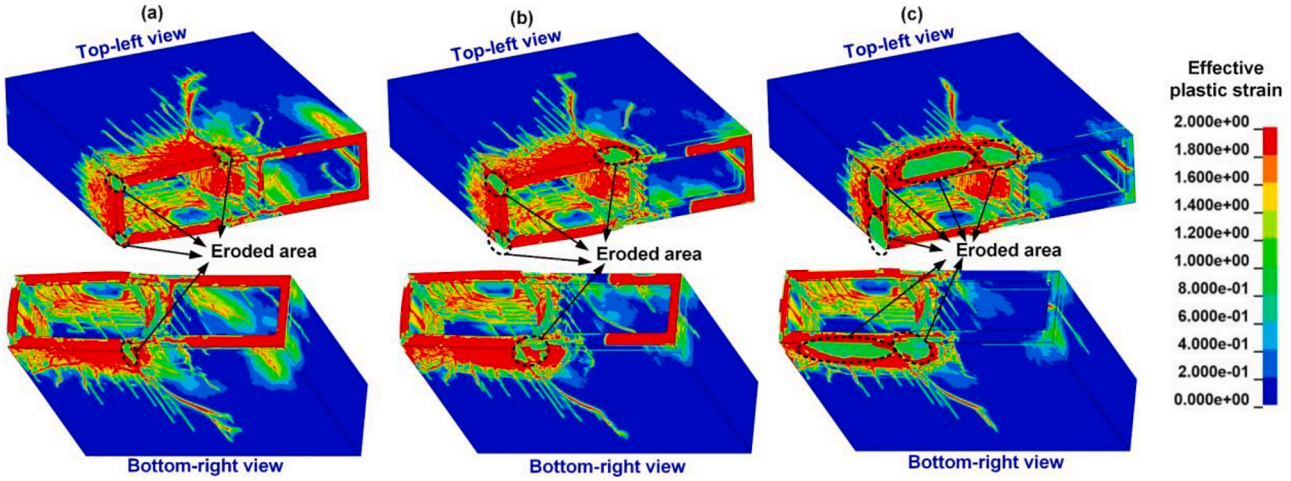

Fig. 23. BLEVE-induced damage of tunnel structures surrounded by the improved soil with thicknesses of (a) 0.5 m, (b) 1 m, and (c) 2 m.

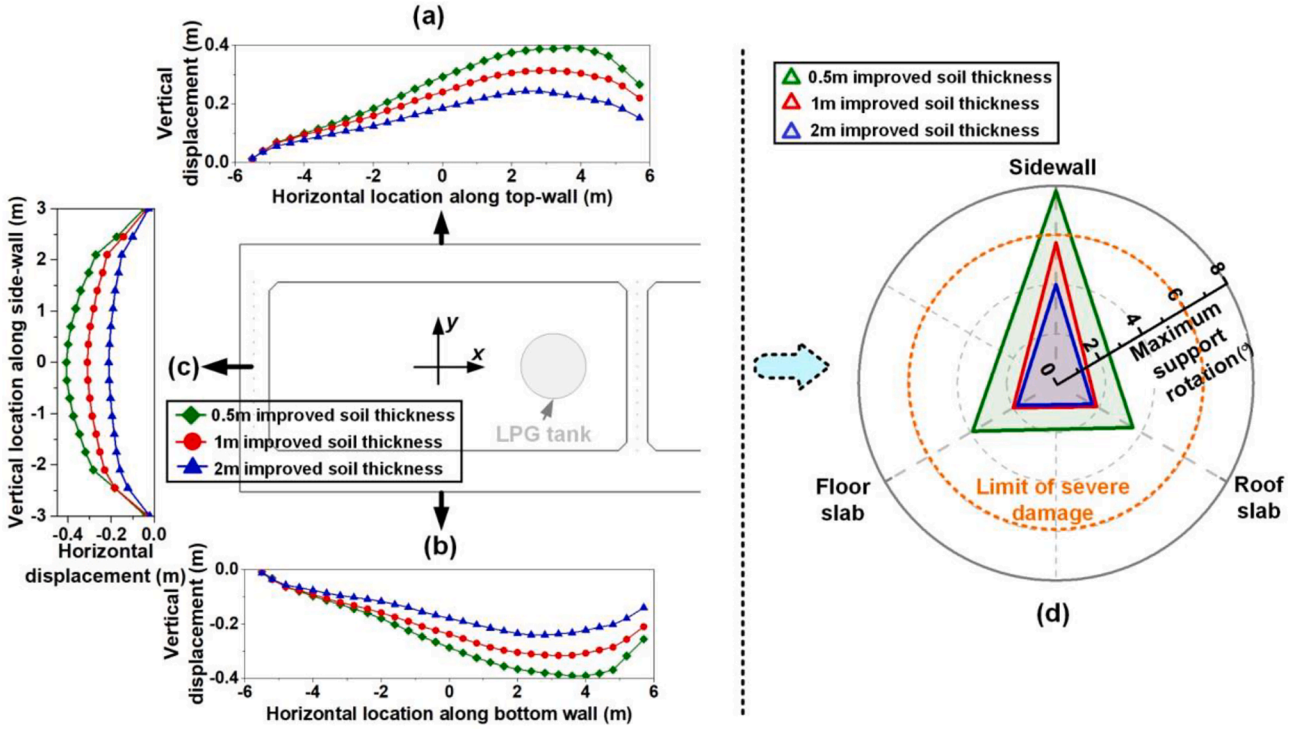

Fig. 24. Peak displacement distribution in the cross-section of BLEVE centre along (a) roof slab, (b) floor slab, and (c) left sidewall surrounded by three thicknesses of improved soil and (d) the corresponding maximum support rotations.

damage under the BLEVE. However, the left sidewall in the case of 0.5 m soil-improvement thickness has the maximum support rotation over 6°, i.e., the left sidewall at the cross-section of BLEVE centre experiences severe damage. Therefore, the improved soil with the soil–cement mixed ratio of 10:0.8 and the thickness of not less than 1 m is suggested to prevent severe damage of the tunnel with the surrounding soil investigated in this study.

It should be noted that although the left roof slab is closer to the LPG tank than the left sidewall, the maximum deformations of the left roof slab and left sidewall are similar as shown in Fig. 24 (a) and (c). It is because only the partial roof slab near the LPG tank (approximately 4 m span along the roof slab above the BLEVE centre) experiences very high BLEVE loads (e.g., the peak overpressure of 17 MPa at the location above the LPG tank filled with 80% liquid), while the remaining part of the roof slab is subjected to much lower BLEVE loads (e.g., the peak overpressure of approximately 3 MPa at the location of the roof slab above the left lane of the tunnel in the case of 80% liquid filling tank) at a delayed time as the blast waves rapidly attenuate with the increased distance from the BLEVE centre and the increased angle of incidence. In addition, the LPG tank is located at the right lane of the tunnel and is closed to the connection of the midwall and the roof slab, which strongly constrains the deformation of roof slab before it collapses. The explosion pressure acting on the left side wall almost uniformly and simultaneously with the peak overpressure of approximately 8 MPa in the case of 80% liquid filling tank and the left sidewall is thinner than the roof slabs. Therefore, the BLEVE-induced maximum deformation of the left sidewall is similar to that of the roof slab although its span length is shorter than the roof slab.

4.2. Effects of soil–cement ratio on tunnel response

In this section, BLEVE-induced damage of tunnel structures surrounded by three soil–cement ratios (i.e., 10:0.1, 10:0.45, and 10:0.8) of improved soil layer with thickness of 1 m is given in Fig. 25. It can be seen that as the amount of cement increases, the damage regions (i.e., red area) of tunnel structures, especially right cell under the BLEVE reduce. It is because as the amount of cement increases, wave impedance of improved soil matches more closely with that of concrete, which causes less stress wave reflection at the interface of soil and concrete and thus less tensile damage of tunnel concrete. However, the eroded areas (i.e., source of fragments) on the outer surfaces of tunnel structures increase with the increased amount of cement. Again, it may be due to the increased compressive action between the interfaces of tunnel structures and surrounding soil, which is caused by the increased inertia effect of improved soil with the increased amount of cement because the soil moves together with the structure owing to the increased soil stiffness.

To determine the effective soil–cement mixture ratio for preventing severe damage of tunnel main structures (i.e., left sidewall, roof slab, and floor slab) under the BLEVE, BLEVE-induced peak displacements and maximum support rotations of tunnel structures at the cross-section of BLEVE centre (i.e., the cross-section experiencing the most severe damage) under three soil–cement ratios of improved soil are shown and compared in Fig. 26. It can be seen that the roof slab and sidewall experience the similar maximum deformation for each case of various soil–cement ratios. The explanation for the similar maximum deformation of the sidewall and roof slab has been given in Section 4.1. In addition, the displacements of tunnel structures at the cross-section of BLEVE centre decrease slightly with the increased amount of cement. It may be because the soil mass can be greatly improved with only small amount of cement addition. However, increasing the amount of cement can enhance the wave impedance of improved soil, thereby reducing the damage (see Fig. 25) due to less tensile stress waves reflected from the interface of soil and concrete. The maximum support rotations of tunnel structures at the cross-section of BLEVE centre under three soil–cement mixed ratios are not much different, as shown in Fig. 26**(d)**. However, the maximum support rotation at the cross-section of BLEVE centre is over 6° when the soil–cement ratio is greater than 10: 0.45. That is, tunnel structures with soil–cement ratio greater than 10:0.45 experience severe damage. Therefore, it is suggested that 1 m thickness of improved soil with soil–cement ratios not greater than 10:0.45, i.e., more cement contents, should be employed to reduce damage of the tunnel under the internal BLEVE.

4.3. Empirical formula for prediction of tunnel support rotation

To provide general design guides and a quick risk assessment for the buried road tunnel against internal BLEVEs, an empirical formula of maximum support rotations of tunnel structures at the cross-section of BLEVE centre is developed in this section as a function of soil–cement mixed properties and BLEVE scenarios. A series of numerical simulations on the buried tunnel surrounded by different thicknesses of improved soil (i.e., 0.5 m, 1 m, and 2 m) and soil–cement ratios (i.e., 10:0.1, 10:0.45, 10:0.6, and 10:0.8) under BLEVEs with two liquid-filling ratios (i.e., 65% and 80%) are conducted. An empirical formula given in Eq. (1) is proposed based on the numerical results of above-mentioned cases by using multivariate nonlinear regression analysis.

$$\theta = 2.5 \times 10^{-3} \times (l_r \times V)^{2.71} \times (r_{sc} \times G_s)^{0.05} \times t_{is}^{-0.42} \quad (1)$$

where θ is the maximum support rotation of structural components of the tunnel (°), l_r is the liquid-filling ratio of LPG tank (%), V is the volume of LPG tank (m^3), r_{sc} is the soil–cement mixture ratio by volume (i.e., soil volume divided by cement volume), G_s is the shear modulus of untreated soil (MPa), t_{is} is the thickness of improved soil layer (m).

Fig. 27 compares the predicted and simulated maximum support rotations of tunnel structures subjected to internal BLEVEs. The coefficient of correlation (R^2) between the simulated data and the predicted results based on Eq. (1) is given along with the mean value of the predicted-to-modelled ratio (M). The predicted support rotations match well with the simulated ones by yielding $R^2 = 0.967$ and $M = 1.012$. Therefore, given the design requirement (i.e., allowable support rotations), Eq. (1) can be used to determine the soil–cement mixed ratio and soil-improved thickness for the protection of buried box-shaped road tunnel against potential BLEVEs occurring inside the tunnel. The empirical formula proposed in this study is established by nonlinearly fitting a series of simulation results. The good correlation coefficient between the simulated and predicted support rotations indicates that the proposed empirical formula can provide the design suggestion for the road tunnel against internal BLEVE within the given ranges, i.e., the tunnel structure, BLEVE scenarios, soil properties, and soil–cement mixture conditions considered in this study.

5. Conclusions

The present study investigates the response of a buried box-shaped road tunnel subjected to internal BLEVEs induced by the burst of a 20 m^3 LPG tank. The effects of soil cover depths, liquid-filling ratios of LPG tank, and BLEVE occurring locations on tunnel response under internal BLEVEs are examined, followed by the comparison of tunnel response

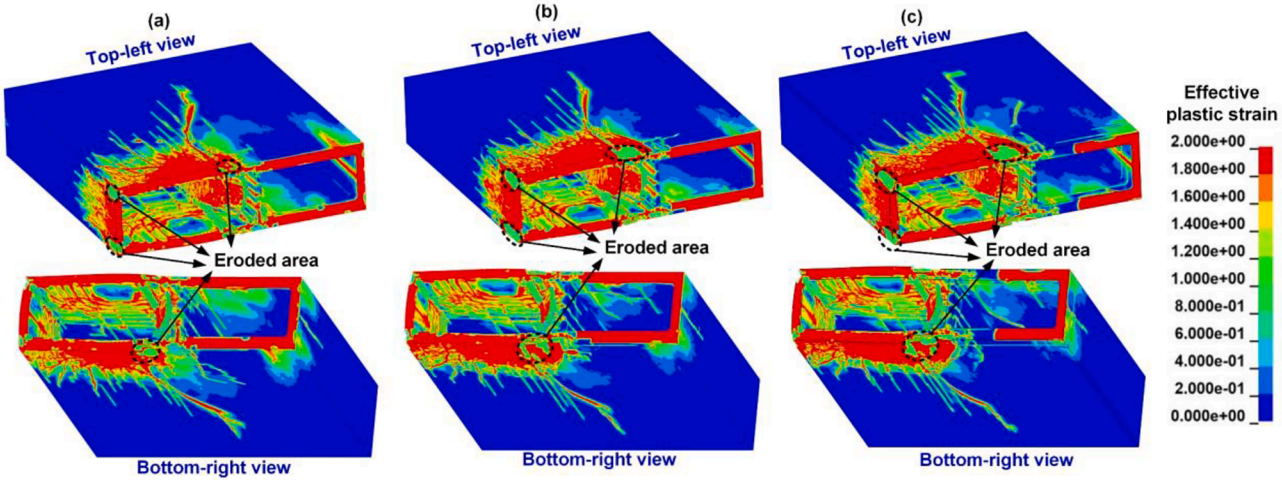

Fig. 25. BLEVE-induced damage of tunnel structures surrounded by improved soil with soil–cement ratios of (a) 10:0.1, (b) 10:0.45, and (c) 10:0.8.

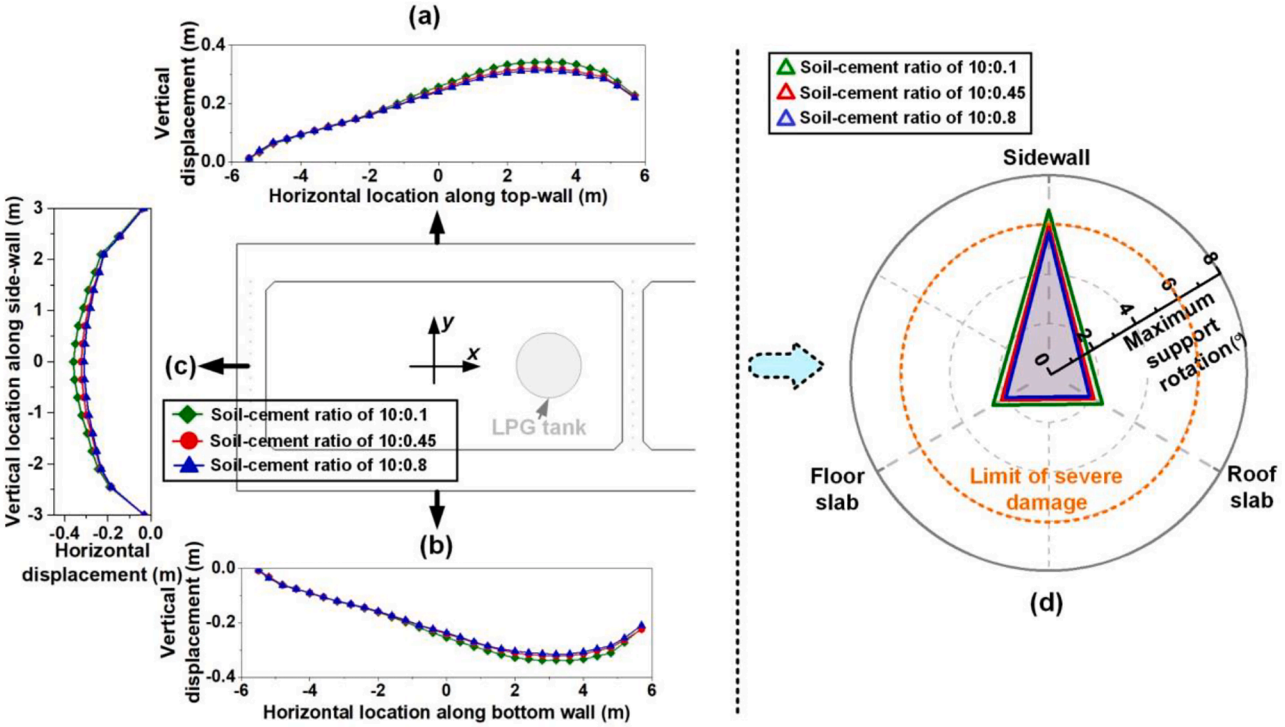

Fig. 26. Peak displacement distribution in the cross-section of BLEVE centre along (a) roof slab, (b) floor slab, and (c) left sidewall surrounded by improved soil with three soil–cement ratios and (d) the corresponding maximum support rotations.

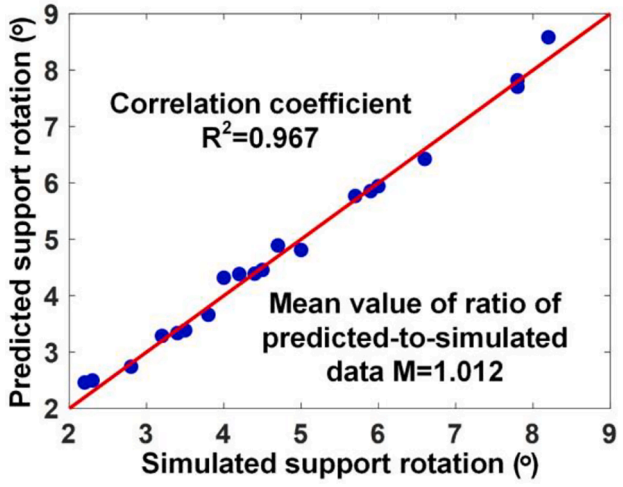

Fig. 27. Comparison of predicted values based on Eq. (1) and simulated data.

under a BLEVE and its equivalent TNT explosion. Furthermore, the performance of improving soil properties by using soil–cement mixture in mitigating BLEVE-induced tunnel response is also examined. The main conclusions are summarized as follows.

(1) The buried box-shaped road tunnel investigated in this study experiences severe damage, even loss of load-carrying capacity under the internal BLEVEs induced by the burst of a 20 m^3 LPG tank filled with liquified gas of 65% or more. Therefore, the LPG tank filled with 65% or more liquid could impose significant risk to the buried road tunnel.
(2) Since the most vulnerable component is the mid-partition wall of the tunnel structure, a simple traffic control of preventing LPG tanks traveling on the lane close to the mid-partition wall could improve the safety of the tunnel.
(3) The TNT-equivalence approach underestimates the impulse of explosion load from BLEVE and hence underpredicts the structural response and damage of the tunnel buried in soil mass.
(4) Improving the properties of sandy soil around tunnel by using cement can reduce the tunnel damage subjected to internal BLEVE.

CRediT authorship contribution statement

Ruishan Cheng: Conceptualization, Methodology, Investigation, Data curation, Formal analysis, Visualization, Writing – original draft. **Wensu Chen:** Conceptualization, Supervision, Validation, Project administration, Writing – review & editing. **Hong Hao:** Conceptualization, Funding acquisition, Supervision, Writing – review & editing. **Jingde Li:** Writing – review & editing.

Declaration of Competing Interest

The authors declare that they have no known competing financial interests or personal relationships that could have appeared to influence the work reported in this paper.

Data availability

Data will be made available on request.

Acknowledgements

The authors acknowledge the financial support from the Australian Research Council (ARC) via Australian Laureate Fellowship (FL180100196).

References

Birk, A.M., Davison, C., Cunningham, M., 2007. Blast overpressures from medium scale BLEVE tests. J. Loss Prev. Process Ind. 20, 194–206.

Bjerketvedt, D., Bakke, J.R., Van Wingerden, K., 1997. Gas explosion handbook. J. Hazard. Mater. 52, 1–150.

Bonalumi, P., Colombo, M., Comina, C., di Prisco, M., Foti, S., Galli, A., 2011a. Characterization of Blast Effects on Surrounding Soil: Internal Detonations in Underground Pipes. Appl. Mech. Mater. 82, 302–307.

Bonalumi, P., Colombo, M., di Prisco, M., 2011b. Internal Explosions in Embedded Concrete Pipes. Appl. Mech. Mater. 82, 452–457.

Bubbico, R., Marchini, M., 2008. Assessment of an explosive LPG release accident: a case study. J. Hazard. Mater. 155, 558–565.

Busch, C.L., Aimone-Martin, C.T., Tarefder, R.A., 2016. Experimental Evaluation and Finite-Element Simulations of Explosive Airblast Tests on Clay Soils. Int. J. Geomech. 16.

Ccps, 2011. Guidelines for Vapor Cloud Explosion, Pressure Vessel Burst, BLEVE, and Flash Fire Hazards. Process. Saf. Prog. 30.

Cheng, R., Chen, W., Hao, H., Li, J., 2021. A state-of-the-art review of road tunnel subjected to blast loads. Tunn. Undergr. Space Technol. 112.

Cheng, R., Chen, W., Hao, H., Li, J., 2022a. Dynamic response of road tunnel subjected to internal Boiling liquid expansion vapour explosion (BLEVE). Tunn. Undergr. Space Technol. 123.

Cheng, R., Chen, W., Hao, H., Li, J., 2022b. Effect of internal explosion on tunnel secondary and adjacent structures: A review. Tunn. Undergr. Space Technol. 126, 104536.

Cheng, R., Chen, W., Li, J.,Hao, H., 2022c. Effects of Cover Depth and Rock Type on Dynamic Response of Road Tunnels Against Internal Explosions. Int. J. Appl. Mech. 2250067.

Chu, C., Zhao, Y., Yi, Y., 2016. Study on an engineering measure to improve internal explosion resistance capacity of segmental tunnel lining structures. J. Vibroengineering 18, 2997–3009.

Consoli, N.C., Foppa, D., Festugato, L., Heineck, K.S., 2007. Key parameters for strength control of artificially cemented soils. J. Geotech. Geoenviron. 133, 197–205.

Di, H., Zhou, S., Yao, X., Tian, Z., 2021. In situ grouting tests for differential settlement treatment of a cut-and-cover metro tunnel in soft soils. Bull. Eng. Geol. Environ. 80, 6415–6427.

Fan, J., Wang, D., Qian, D., 2018. Soil-cement mixture properties and design considerations for reinforced excavation. J. Rock Mech. Geotech. Eng. 10, 791–797.

Feldgun, V.R., Kochetkov, A.V., Karinski, Y.S., Yankelevsky, D.Z., 2008. Internal blast loading in a buried lined tunnel. Int. J. Impact Eng. 35, 172–183.

Hu, Z.F., Yue, Z.Q., Zhou, J., Tham, L.G., 2003. Design and construction of a deep excavation in soft soils adjacent to the Shanghai Metro tunnels. Can. Geotech. J. 40, 933–948.

Lea, C.J., 2002. A review of the state-of-the-art in gas explosion modelling, HSL/2002/02.

Lee, W.Y., 2006. Numerical modeling of blast-induced liquefaction. Brigham Young University.

Lewis, B.A., 2004. Manual for LS-DYNA soil material model 147, FHWA-HRT-04-095.

Li, H., Chen, W., Hao, H., 2019. Influence of drop weight geometry and interlayer on impact behavior of RC beams. Int. J. Impact Eng. 131, 222–237.

Li, J., Hao, H., Chen, W., Cheng, R., 2022. Calculation of BLEVE energy and overpressures inside a tunnel using analytical and CFD methods. Tunn. Undergr. Space Technol. 120.

Livermore Software, T., 2020. LS-DYNA keyword user's manual, R12.

Meng, Q., Wu, C., Li, J., Liu, Z., Wu, P., Yang, Y., Wang, Z., 2020. Steel/basalt rebar reinforced Ultra-High Performance Concrete components against methane-air explosion loads. Compos. B, Eng, p. 198.

Ministry of Transport of the People's Republic of China, 2018. Specifications for design of highway tunnels section 1 Civil engineering, JTG 3370.1-2018.

Nicolini, E., Nova, R., 2000. Modelling of a tunnel excavation in a non-cohesive soil improved with cement mix injections. Comput. Geotech. 27, 249–272.

Origin-Energy, 2015. LPG Gas Cylinder Sizes and Applications, https://www.originenergy.com.au/wp-content/uploads/LPG-cylinder-sizes.pdf.

Ouyang, Z., Carlton, A., Guo, Q., Naito, C.,Quiel, S., 2020. Blast Vulnerability of Drop Ceilings in Roadway Tunnels. J. Perform. Constr. Facil. 34.

Phulari, V.S.,Goel, M.D., 2021. Dynamic response of tunnel under blast loading and its blast mitigation using CFRP as protective barrier, Recent Advances in Computational Mechanics and Simulations. Springer, Singapore, pp. 555–562.

Prugh, R.W., 1991. Quantitative evaluation of" bleve" hazards. J. Fire Prot. Eng. 3, 9–24.

Qian, H., Li, J., Zong, Z., Wu, C., Pan, Y., 2021a. Behavior of precast segmental utility tunnel under ground surface Explosion: A numerical study. Tunn. Undergr. Space Technol. 115.

Qian, H., Zong, Z., Wu, C., Li, J., Gan, L., 2021b. Numerical study on the behavior of utility tunnel subjected to ground surface explosion. Thin-Walled Struct. 161.

Suazo, G., Villavicencio, G., 2018. Numerical simulation of the blast response of cemented paste backfilled stopes. Comput. Geotech. 100, 1–14.

Tiwari, R., Chakraborty, T., Matsagar, V., 2018. Analysis of curved tunnels in soil subjected to internal blast loading. Acta Geotech. 15, 509–528.

To, C.W., Chow, W.K., Cheng, F.M., 2021. Numerical studies on explosion hazards of vehicles using clean fuel in short vehicular tunnels. Tunn. Undergr. Space Technol. 107.

US Department of Defense, 2008. Structures to resist the effects of accidental explosions, UFC 3-340-02.

US Department of Transportation Federal Highway Administration, 2009. Technical manual for design and construction of road tunnels — civil elements, FHWA-NHI-10-034.

van den Berg, A.C., van der Voort, M.M., Weerheijm, J., Versloot, N.H.A., 2006. BLEVE blast by expansion-controlled evaporation. Process. Saf. Prog. 25, 44–51.

van den Berg, A.C., Weerheijm, J., 2006. Blast phenomena in urban tunnel systems. J. Loss Prev. Process Ind. 19, 598–603.

Vervuurt, A.H.J.M., Galanti, F.M.B., Wubs, A.J.,Van den Berg, A.C., 2007. Effect of explosions in tunnels-Preliminary assessment of the structural response, 2007-D-R0156/A.

Wei, X.Y., Zhao, Z.Y., Gu, J., 2009. Numerical simulations of rock mass damage induced by underground explosion. Int. J. Rock Mech. Min. Sci. 46, 1206–1213.

Yang, G., Wang, G., Lu, W., Yan, P., Chen, M., 2019. Damage assessment and mitigation measures of underwater tunnel subjected to blast loads. Tunn. Undergr. Space Technol. 94.

Yu, H., Wang, Z., Yuan, Y., Li, W., 2015. Numerical analysis of internal blast effects on underground tunnel in soils. Struct. Infrastruct. Eng. 12, 1090–1105.

Zhao, H., Yu, H., Yuan, Y., Zhu, H., 2015. Blast mitigation effect of the foamed cement-base sacrificial cladding for tunnel structures. Constr. Build. Mater. 94, 710–718.